DISASTER RISK REDUCTION IN MALAYSIA AND EARTHQUAKE STUDY BASED ON CYCLIC TRIAXIAL TEST

CHIENG TZE SHENG, ALEXANDER

A project report submitted in partial fulfilment of the requirements for the award of Bachelor of Engineering (Hons.) Civil Engineering

Faculty of Engineering and Science
Universiti Tunku Abdul Rahman

May 2013

DECLARATION

I hereby declare that this project report is based on my original work except for citations and quotations which have been duly acknowledged. I also declare that it has not been previously and concurrently submitted for any other degree or award at UTAR or other institutions.

Signature : ____________________

Name : Chieng Tze Sheng, Alexander

ID No. : 09UEB07674

Date : ____________________

APPROVAL FOR SUBMISSION

I certify that this project report entitled **"DISASTER RISK REDUCTION IN MALAYSIA AND EARTHQUAKE STUDY BASED ON CYCLIC TRIAXIAL TEST"** was prepared by **CHIENG TZE SHENG, ALEXANDER** has met the required standard for submission in partial fulfilment of the requirements for the award of Bachelor of Engineering (Hons.) Civil Engineering at Universiti Tunku Abdul Rahman.

Approved by,

Signature : ______________________________

Supervisor : Prof. Dr Yasuo Tanaka

Date : ______________________________

Specially dedicated to

my beloved grandparents, mother and father

ACKNOWLEDGEMENTS

I would like to thank everyone who had contributed to the successful completion of this project. I would like to express my gratitude to my research supervisor, Prof. Dr Yasuo Tanaka for his invaluable advice, guidance and his enormous patience throughout the development of the research.

In addition, I would also like to express my gratitude to my loving parent and friends who had helped and given me encouragement since the first day of this research till the end. Without all these people, this research will not come to a success.

DISASTER RISK REDUCTION IN MALAYSIA AND EARTHQUAKE STUDY BASED ON CYCLIC TRIAXIAL TEST

ABSTRACT

Malaysia is tectonically situated in the relatively stable Subdaland. However, Malaysia can still experience tremors from the earthquakes generated from neighbouring country. In this research, cyclic triaxial is used to study the dynamic properties of residual soil. Before running the cyclic loading, the soil is classified with a few test, namely wet sieve analysis, Atterberg limit test, compaction test, and in-situ density test. Next, the cyclic triaxial system is also set up by putting together the loading frame, control panel, triaxial cell, sensors, and programs to acquire data and control the cyclic loading. Calibrations are carried out on all the sensors required in this research. This report presents the data obtained from the cyclic triaxial test of compacted residual soil with a density of 16kN/m^3, and the author concluded that the frequency did not affect greatly the shear modulus and damping ratio. The results of cyclic triaxial test on compacted residual soil with a density of 15 kN/m^3 will be presented by Boon (2013). On the other hand, the shear modulus decreased with the increase of stress ratio, whereas damping ratio increased with the stress ratio. Other than that, the graph of shear modulus vs shear strain and damping ratio vs shear strain is obtained. Plus, the author also concluded that the Local Deformation Transducer (LDT) is more reliable than Linear Variable Displacement Transformer (LVDT).

TABLE OF CONTENTS

LIST OF TABLES

LIST OF FIGURES

LIST OF SYMBOLS / ABBREVIATIONS

a	air pressure, kPa
A	constant
A_{loop}	area of hysterical loop
$A_{triangle}$	area of triangle
A_0	initial area, m^3
A_1	new area, m^3
D	damping ratio
E	young modulus, kPa
$F(e)$	function of e
G	shear modulus, kPa
G_0	initial shear modulus, MPa
G_1	new shear modulus, MPa
m	mass, kg or g
n	constant
s	strain
SR_1	stress ratio at first point
SR_2	stress ratio at second point
v	voltage, V
γ	shear strain
ε_1	axial strain of first point
ε_2	axial strain of second point
ε_a	axial strain
σ_d	deviatoric stress, kPa
σ_c	consolidation pressure, kPa

σ_{c0}	initial confining pressure, MPa
σ_{c1}	new confining pressure, MPa
σ_1	stress of first point, kPa
σ_2	stress of second point, kPa
μ	poisson ratio

BT	Bukit Timah Granite
JF	Jurong Formation
LDT	local deformation transducer
LVDT	linear variable displacement transformer
MMI	modified mercalli intensity
MMD	Malaysian meteorological department

LIST OF APPENDICES

CHAPTER 1

INTRODUCTION

1.1 Background of Study

Malaysia is located on the Sundaland, which is relatively stable from earthquake. (Sherliza et. al, 2012). This does not mean that Malaysia is free from earthquake tremors generated locally and from neighbouring country. The highest recorded Modified Mercalli Intensity Scale (MMI) in West Malaysia is VI, whereas for East Malaysia is VII. The scale of VII is able to produce a moderate damage to well-built ordinary structures and a considerable amount of damage to poorly-built structures. However, less than one percent of buildings in Malaysia are seismic resistant (Taksiah Abdul Majid, 2009).

To design any geotechnical engineering problems that involve dynamic loading of soils and soil-structure interaction systems requires the determination of two important parameters, the shear modulus and the damping ratio of the soils (Sitharam, 2004). In this research, these two parameters are obtained from the soil sampled from Shah Alam, Selangor.

In addition, the data for the dynamic properties of soil in Malaysia is very rare as there are not many researchers in Malaysia is studying about these dynamic properties. Therefore, more of these researches should be done in Malaysia to provide a large database in order to improve the structure and to reduce the disaster risk in Malaysia.

1.2 Aims and Objectives

The aim of this project is to obtain the dynamic properties of the soil obtained from Alam Impian, Shah Alam, Selangor, with the coordinate of 3°1'36.23"N, 101°30'57.36"E. The specific objectives are set forth:

i. To classify the soil collected from the site.
ii. To set up the cyclic triaxial system.
iii. To obtain the shear modulus and damping ratio of the soil.
iv. To plot a graph of shear modulus vs. shear strain and damping ratio vs. shear strain.

1.3 Layout of Report

This thesis is divided into five chapters. The first chapter describes about the background study, aims and objectives, significance of study and the layout of report. On the other hand, the second chapter deals with the vulnerability and seismic activity in Malaysia, the advantages and disadvantages of cyclic triaxial test, the factors affecting dynamic properties, the comparison between dynamic compaction and static compaction, and the dynamic properties of residual soil in Singapore.

Furthermore, the third chapter explains about the research methodology. This chapter describes every steps in detail for soil sampling, soil classification, set up of cyclic triaxial system, calibrations, and the testing of the sample. Next, the fourth chapter deals with about the results and discussion. This chapter shows and discusses the dynamic properties obtained from the test and also the problems encountered. Lastly, the fifth chapter presents the conclusions and the future recommendations for this research.

CHAPTER 2

LITERATURE REVIEW

2.1 Introduction

This chapter presents the vulnerability and seismic activity in Malaysia, the advantages and disadvantages of cyclic triaxial test, the factors affecting dynamic properties, the comparison between dynamic compaction and static compaction, and the dynamic properties of residual soil in Singapore.

2.2 Vulnerability and Seismic Activity in Malaysia

Malaysia is a country that falls under low seismicity group and a seismotectonic study has been conducted by the Mineals and Geoscience Department of Malaysia (MGDM) that confirms Malaysia is tectonically situated in the relatively stable Subdaland (Sherliza et. al, 2012). However, it does not mean that Malaysia is free from earthquake threat because it lies close to Sumatran faut and Sumatran Subduction zone. Huge earthquakes that originated from these two active areas did create considerably ground motion over western part of West Malaysia.

On 4 June 2000, Bengkulu Earthquake occurred in the Sumatran subduction zone had shook several buildings in Johor Bahru and Klang Valley. Minor cracks in the building wall was reported in Johor Bahru and the maximum observed intensity in Johor Bahru and Kuala Lumpur was estimated of about VI on Modified Mercalli Intensity (MMI) scale (Rosaidi, 2001).

Whereas, the Sumatran Fault ruptured at magnitude of about 7.0 on Richter Scale in the 1995 and about 450km away from Johor. This also has an intensity of VI on MMI scale. In addition, the 1996 event with magnitude of about 5.4 on Richter Scale and about 300km from coast of Perak also shook many high-rise buildings in Penang, Perak, Kuala Lumpur and Selangor. The observed intensity was also VI on MMI scale (Rosaidi, 2001).

On the other hand, East Malaysia is classified as moderately active in seismicity. Sabah is the only state that has the most earthquake activities in Malaysia. The maximum observed intensity in Lahad Datu and Kunak was estimated of about VII on MMI scale. Other than that, Sarawak also experienced several earthquakes of local origin. Over the last 35 years, a total of three earthquake occurred in Sarawak with maximum observed intensity of IV on MM scale. Besides, these two states also affected by earthquake originated from Southern Philippine, Makassar Strait, Sulu Sea and Celebes Sea (Rosaidi, 2001).

Based on the information obtained from the Malaysian Meteorological Department (MMD), the maximum recorded MMI scale from 1875 to 2011 for East Malaysia is VII, whereas the largest recorded MMI scale from 1909 to 2011 for West Malaysia is VI. This data is shown in the two figures below.

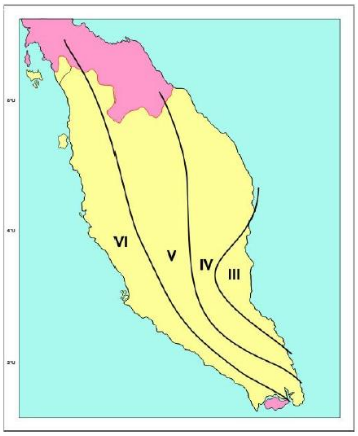

Figure 2.1: Maximum Observed Earthquake Intensity (MMI Scale) for Peninsular Malaysia from MMD

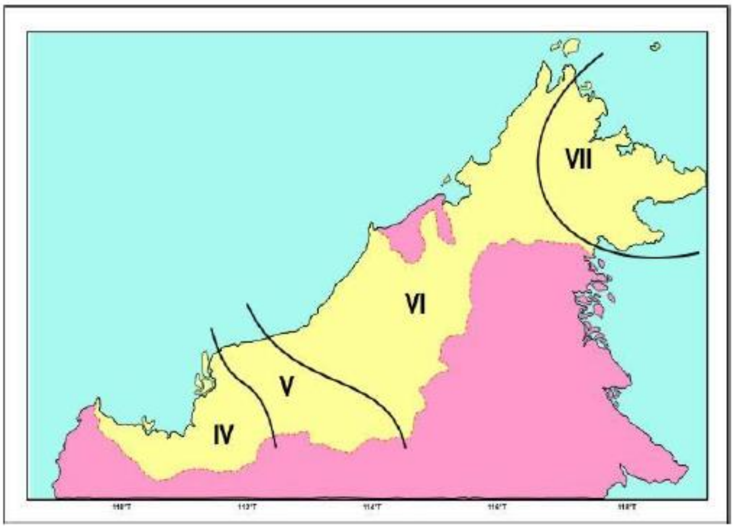

Figure 2.2: Maximum Observed Earthquake Intensity (MMI Scale) for Sabah and Sarawak from MMD

According to the MMI scale description, for the scale of VII, which is the highest recorded MMI scale in Malaysia, it states that there will be a moderate damage occur to well-built ordinary structures and also considerable amount of damage in poorly built or badly designed structures. However, less than one percent of buildings in Malaysia are seismic resistant (Taksiah Abdul Majid, 2009).

On the other hand, the table from Sherliza et al (2012) summarized the frequency and intensity of felt earthquakes recorded from 1874 to 2010 for every states in Malaysia is shown below.

Table 2.1: Frequency and Intensity of Felt Earthquakes Recorded from 1874 to 2010 (Sherliza et al, 2012)

State	Frequency of Occurrence	Maximum Intensity (MMI)
Peninsular Malaysia (1909 – July 2010)		
Perlis	3	V
Kedah	18	V
Penang	41	VI
Perak	24	VI
Selangor	50	VI
Negeri Sembilan	14	V
Malacca	19	V
Johor	32	VI
Pahang	35	III
Terengganu	2	IV
Kelantan	3	IV
Kuala Lumpur/Putrajaya	38	VI
East Malaysia		
Sabah (1897- July 2010)	40 (77)*	VII
Sarawak (1874 – July 2010)	17 (21)**	VI

*Frequency of occurrence recorded as 40 by MMD, but reported as 77 by MOSTI (2009)

**Frequency of occurrence recorded as 17 by MMD, but reported as 21 by MOSTI (2009)

This shows that Malaysia is quite vulnerable to earthquake. Therefore, more research should be done in Malaysia to provide a large database of earthquake related information, which will be useful for the purpose of disaster risk reduction.

2.3 Advantages and Disadvantages of Cyclic Triaxial Test

There are a few advantages and disadvantages of this cyclic triaxial test. In the past 40 years, most of the liquefaction testing of sands, silts, and even low plasticity clays has been performed using this triaxial equipment. Therefore, there is a large database of information accumulated throughout these years of testing. This has benefited the engineering community by improving the ability to draw rational conclusions on the cyclic response of untested materials by comparing responses of other soils within the database (Jennifer et al, 2007).

The main disadvantage of this triaxial test is that it does not reflect the actual field conditions. The earthquake motion replicated with this equipment is not vertically propagating horizontal shear waves, but a cyclic vertical loading. Besides, the specimens are typically isotropically consolidated, whereas the soil in the field is usually anisotropically consolidated. In addition, the rotation of the principal stresses during loading is also different. The direction of the major principal stress in triaxial test will instantaneously rotate 90º from vertical to horizontal and then back. However, the major principal stress will rotate smoothly and remain nearly vertical in the field (Jennifer et al, 2007).

Another problem with the triaxial cyclic test it the occurrence of "necking" during the extension phase of loading. The term, "necking" defines as the local decrease in cross-sectional area, which induces significant stress concentrations. When significant stresses are induced, the experimental stress-strain measurements will be affected due to the inconsistency of the global volume throughout the specimen. (Jennifer et al, 2007).

In addition, the cyclic triaxial used in this research is using a sensor called Local Deformation Transducer (LDT). This sensor is able to measure up to around 10^{-5} to 10^{-6} of strain, which is beyond what many other sensors can do, such as the Linear Variable Displacement Transformer (LVDT). This LDT functions based on the concept of Wheatstone bridge. A Wheatstone bridge is a network of four resistive legs. One or more of these legs and the below shows the Full-Bridge configuration. In this research, the LDT is constructed by using the Full-Bridge configuration, where four strain gauges are used. The procedure of fabricating this LDT is explained in Chapter 3.

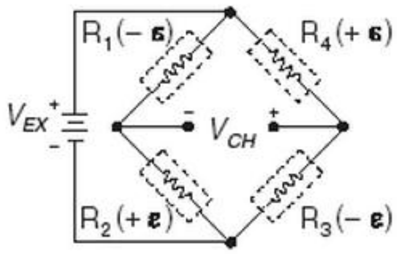

Figure 2.3: Full-Bridge Configuration

2.4 Factors Affecting Dynamic Properties

In order to evaluate the reaction of foundations subjected to vibrations and the manner of vibrations and its transmission through the soil, the dynamic properties of the soil must be determined (T.G. Sitharam et al, 2004). There are several factors that affect the dynamic properties of soil, especially the shear modulus and damping ratio. Many researches have been conducted in the past by experts around the world and their conclusions are explained below.

Hardin and Richart (1963) (in Martin, 1990) conclude that the shear modulus of sand varied with the square root of the isotropic confining pressure. Besides, they also proved that the void ratio was one of the most significant variables affecting shear modulus, along with other properties like moisture content, grain characteristics, and gradation influencing the modulus mainly by how they affect void ratios.

On the other hand, Hardin and Black (1966) (in Martin, 1990) concludes that the stress modulus of normally consolidated clay also proportional to the square root of the confining pressure. Plus, they also concluded that the function relationship for shear modulus would include many factors such as effective octahedral normal stress, void ratio, ambient stress and vibration history, degree of saturation, octahedral shear stress, grain characteristics, grain shape, grain size, grading, mineralogy, amplitude of vibration, frequency of vibration, secondary effects that are a function of time, soil structure, and temperature, including freezing.

In addition, Hardin and Black (in Martin, 1990) also stated that the mean effective stress, void ratio and strain amplitude are the most important factors affecting shear modulus. The degree of saturation and overconsolidation ratio were also important for cohesive soils, but appeared less important for sands.

The damping values are affected by the same factors that influence the shear modulus. The difference is that damping is affected oppositely of shear modulus. In other words, as the shear modulus increases, the damping will decrease and vice versa. In an ideal condition, the maximum damping value can be archived when shear modulus is equal to zero (Pieter, 1992).

2.5 Sample Preparation by Static Compaction

In this research, static compaction is used to prepare the soil sample for testing. The difference between statically or dynamically compacting sample affects the test results on soil properties. A static compaction will produce a soil sample that is stiffer, stronger and less plastic compared to specimen produced from dynamic compaction (Doris and Hafez, 2011).

Besides, the static compaction also gives a higher shear strength value. This is shown in the table below by Doris and Hafez.

Table 2.2: Summary of Shear Strength Value for all Soil (Doris and Hafez, 2011)

Soil Sample	Shear Strength (kPa)	
	Static	Dynamic
A	366.5	327.0
B	279.5	115.0
C	422.5	204.5
D	399.5	153.0
E	260.5	98.0
F	556.0	489.5
G	395.5	116.5

Plus, Doris and Hafez also concluded that the specimen produced by the dynamic compaction is not uniform when compacted to static compacted specimen. They had tested the soil specimen with X-ray test and the result are shown in the below.

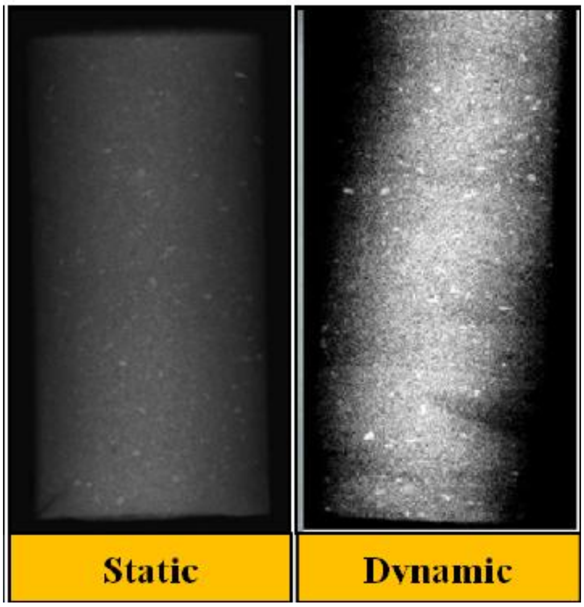

Figure 2.4: X-ray Photo for Dynamic and Static Compacted Soil

Therefore, the static compaction method is used in this research to prepare the samples with different degrees of compaction to correlate with field data. In addition, this method is also faster, easier and simpler to be carried out in the laboratory compared to dynamic compaction method.

2.6 Dynamic Properties of Residual Soil in Singapore

In Singapore, the dynamic properties of residual soil have been studied by cyclic triaxial test. Tou (2003) has studied the dynamic properties of two different Singapore soils and they are the Jurong Formation residual soils and Bukit Timah Granite residual soil.

Tou (2003) shows that the shear modulus of the soil decreases with the increase in shear strain and the damping ratio increasing with the increase of shear strain. Additionally, he shows that the shear modulus and damping ratio at certain shear strain level increase as the frequency increases. This is more obvious at small shear strain levels like 0.01 %, 0.02 % and 0.03 % (Tou, 2003).

Plus, by comparing the normalized shear modulus and damping ratio for saturated sand and clays show that the dynamic properties of the test specimen fall in the average range of saturated sand, whereas the damping ratio of the specimen is higher compared to those of saturated sand (Tou, 2003).

In addition, Tou (2003) also compared the normalized shear modulus of the soil sample with those of Piedmond residual soils. It does not show a great variation with the average trend of Piedmond residual soils. However, the damping ratio of the residual soil specimen shows a higher value in comparison (Tou, 2003).

Besides, the shear moduli determined 'locally' by using a pair of Local Deformation Transducer (LDT) generally show higher values compared with the shear modulus determined 'externally' using the Linear Variable Displacement Transformer (LVDT) especially at small shear strain levels like 0.01 %, 0.02 % and 0.03 %. This shows the importance of local strain measurement in cyclic triaxial test (Tou, 2003). The results by Tou (2003) are further discussed in Chapter 4.

CHAPTER 3

METHODOLOGY

3.1 Introduction

This chapter explains the methodology of every activities done throughout this whole research such as the soil sampling method, soil classification, set up of cyclic triaxial system, calibration of sensors and air pressure, and the cyclic triaxial testing procedure.

3.2 Soil Sampling

Firstly, a soil testing company, Sealand Teknikal Sdn Bhd, is contacted by the author's research supervisor. Then a site in Shah Alam, Selangor, with the coordinate 3°1'36.23"N, 101°30'57.36"E is recommended by the soil testing company. After the site visitation by the author's research supervisor, the location is decided and preparation for soil sampling is started.

Two types of soil are obtained from the site, namely the undisturbed and disturbed residual soils. For collecting undisturbed sample, the following procedures are used. First, the top layer of the soil being removed and flattened to place a wooden plate for soil nail sampling. By hammering the 23 cm long nails along the plate into the ground, a block of undisturbed soil is securely held in position so that this soil block can be excavated from the rest of the soil. These nails also act as a support for the soil once the soil is taken out.

Figure 3.1: Hammering the Twelve Nails into the Soil

Once the soil sample is taken out, it is then carefully overturned and a layer of plaster is pasted on the whole soil sample. Thus the soil was kept undisturbed and prevented from the loss of moisture. Then the soil is transported to laboratory by being wrapped by air bubble sheet.

Figure 3.2: Plastering of the Undisturbed Soil Sample

Additionally, disturbed residual soil was collected by simply excavating the ground and transported to laboratory in a bag. Disturbed soil is dried under the sun and then physical and compaction tests were carried out by using air-dried sample. For this current Final Year Project research, only the disturbed samples are used and the undisturbed samples are kept for the future research.

3.3 Soil Classification Tests

This section presents the results of the wet sieve analysis, Atterberg limits test using cone penetrometer and compaction test based on the procedure from BS 1377.

3.3.1 Wet Sieve Analysis

The table below shows the data obtained from wet sieve analysis and a graph of percentage of finer vs particle size is plotted and shown as well.

Table 3.1: Wet Sieve Data

Mesh Aperture (mm)	Mass of Tray (g)	Mass of Tray with Soil (g)	Mass of Soil Retained (g)	Mass of Soil Retained (%)	Cumulative of coarser (%)	Cumulative of finer (%)
2.000	36.3	36.8	0.5	0.250	0.250	99.750
1.180	53.7	61.2	7.5	3.750	4.000	96.000
0.600	34.3	55.9	21.6	10.800	14.800	85.200
0.425	34.3	56.4	22.1	11.050	25.850	74.150
0.300	34.7	49.9	15.2	7.600	33.450	66.550
0.212	34	53.4	19.4	9.700	43.150	56.850
0.150	34.3	68.2	33.9	16.950	60.100	39.900
0.063	36.2	66.7	30.5	15.250	75.350	24.650
receiver			49.3	24.650	100.000	0.000
		Total	200	100.000		

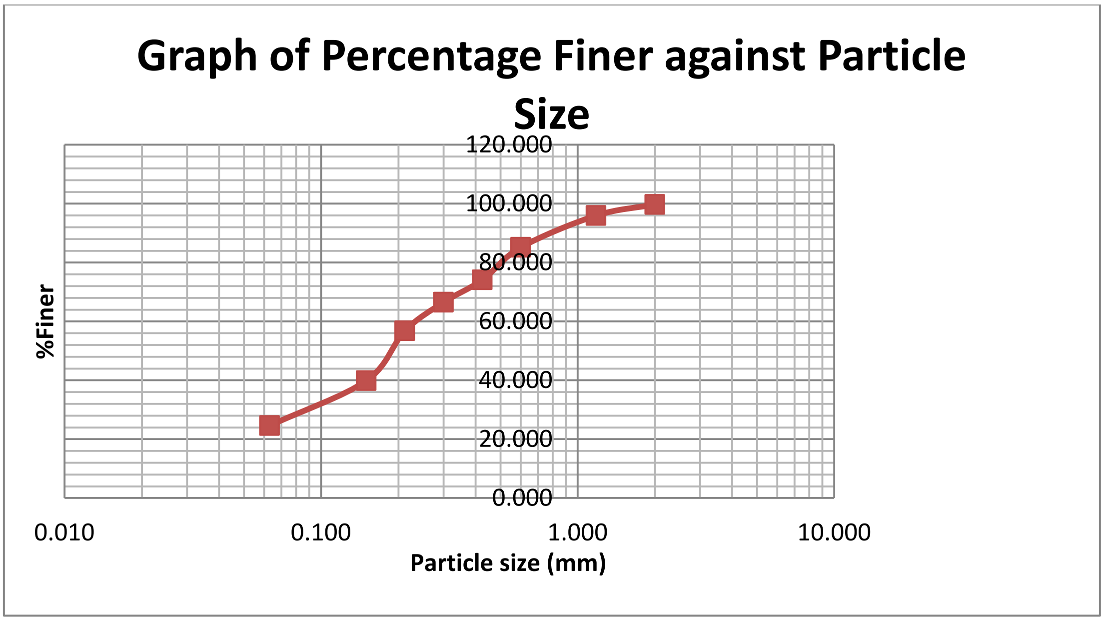

Figure 3.3: Graph of percentage of finer vs particle size

From the graph above, less than 35 % of the material is finer than 0.063 mm and more than 50 % of coarse material is of sand size (finer than 2mm). Based on BS 5930.81, this soil is categorised under sand.

3.3.2 Atterberg Limit Test

The table below shows the data obtained from the Atterberg Limit Test with cone penetrometer. The label LL is for liquid limit test, whereas label with PL is for plastic limit test.

Table 3.2: Atterberg Limit Test Data (Part 1)

Label	Mass of Tray (g)	Mass of Tray with Moisture soil (g)	Mass of Moisture soil (g)	Penetration value (mm)
LL1	34.1	36.6	2.5	16.8
LL2	33.7	39.3	5.6	17
LL3	33.8	40.7	6.9	19.8
LL4	34.4	40.4	6	22.5
LL5	35.5	45.5	10	23.7
PL	33.9	36.1	2.2	-

Table 3.3: Atterberg Limit Test Data (Part 2)

Label	Mass of Tray with Dried soil (g)	Mass of dried soil (g)	Mass Moisture Content (g)	Moisture content (%)
LL1	35.7	1.6	0.9	56.25
LL2	37.3	3.6	2	55.56
LL3	38.1	4.3	2.6	60.47
LL4	38	3.6	2.4	66.67
LL5	41.4	5.9	4.1	69.49
PL	35.6	1.7	0.5	29.41

In addition, graph of water content vs penetration is plotted and the liquid limit is obtained. This graph is shown in the below.

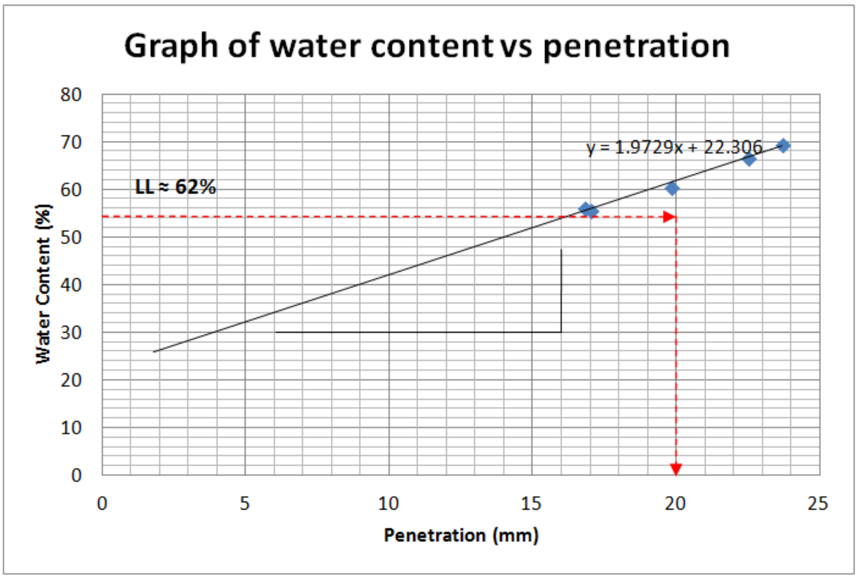

Figure 3.4: Graph of Water Content vs Penetration

The result shows that the liquid limit of the soil is 62 % and the plastic limit is 29.41 %. Therefore, the plasticity index of the soil is 32.35 %. Based on the plasticity chart obtained from the British standard (BS 5930, 1999), the soil falls under MH category. From the British soil classification system (BS 5930.81, the soil falls under the category of very silty sand and the symbol is SMH.

3.3.3 Compaction Test

The table below shows the data obtained from this test. Next, graph of dry density vs moisture content is also plotted and shown below. The highlighted value in the table is the dry density and the water content at the peak of the graph.

Table 3.4: Compaction Test Data

Moisture content before compaction (%)	11.00	14.00	17.00	20.00	23.00
Mass of mould (g)	4206.30	4207.30	4206.20	4208.50	4206.00
Mass of mould & compacted soil, m2 (g)	5888.80	6081.90	6222.80	6196.20	6176.70
Mass of tray (g)	34.00	34.10	33.80	33.90	34.60
Mass of tray & moist soil (g)	138.20	144.70	144.30	184.00	117.20
Mass of moist soil (g)	104.20	110.60	110.50	150.10	82.60
Mass of tray & dry soil (g)	126.90	130.70	128.10	158.60	101.40
Moisture content after compaction (g)	11.30	14.00	16.20	25.40	15.80
Moisture content after compaction, w (%)	10.84	12.66	14.66	16.92	19.13
Bulk density, ρ (Mg/m3)	1.68	1.87	2.02	1.99	1.97
Dry density, ρd (Mg/m3)	1.52	1.66	1.76	1.70	1.65

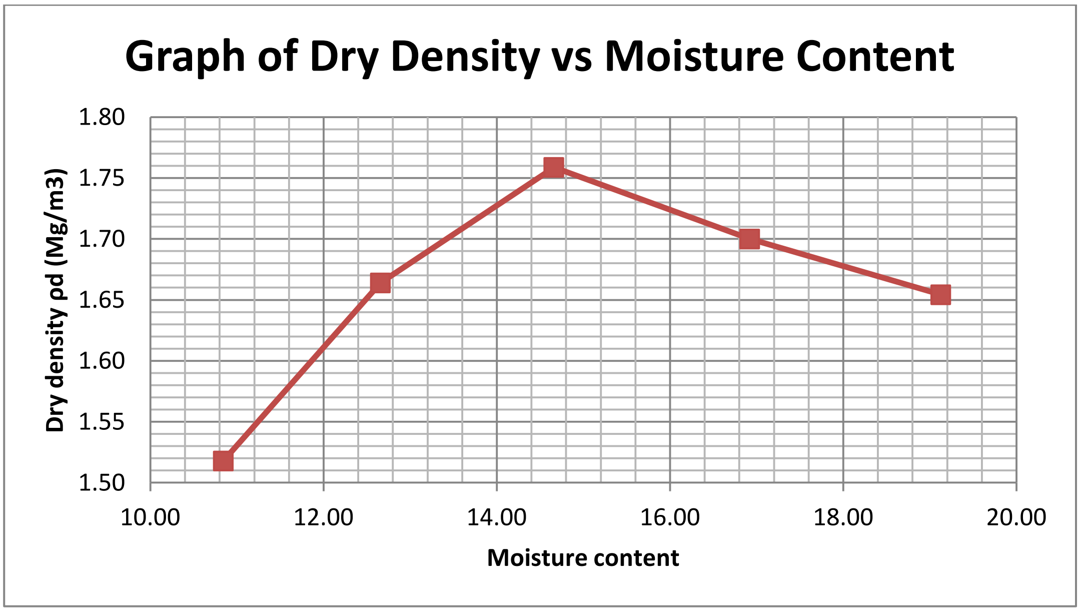

Figure 3.5: Graph of Dry Density vs Moisture Content

In conclusion, the maximum dry density with the value of 1.76 Mg/m^3 falls on the water content of 14.66 %.

3.3.4 In-Situ Density Test

In-Situ Density Test is carried out in the site itself to determine the density of the soil at the site. This can be done by first flattening the soil surface. Then, a square cardboard with a hole in the middle is placed on it and held firmly. The hole must be big enough for the soil sampler to pass through. The purpose of this cardboard is to act as a guide and to prevent the soil that is going to be dug out to be mixed up with the surrounding soil. After that, soil is dug out from the hole carefully with a small spade and soil sampler, making sure that the all soil that is dug out from the hole is collected in a bag and labelled.

Figure 3.6: Obtaining the Soil Sample

Next, a plastic bag is placed in the hole and water is poured in until it reached the surface. Hand is used to push the plastic to the soil surface in the hole to make sure that the water in the plastic bag covered all the void in the hole. After that, the plastic bag is removed from the hole, tied properly and labelled. The above test is repeated few more times on two different location, namely Site A and Site B.

Figure 3.7: Water is Poured into the Hole

The volume of water in the plastic bag is measured and recorded immediately after the plastic bag is taken out from the hole, whereas the soil samples collected are brought back to the laboratory to be weighted and dried. Then, the moisture content and density is calculated. The data obtained from this test is shown below.

Table 3.5: In-Situ Density Test Data (Part 1)

Sample	Volume (ml)	Mass of Tray (g)	Mass of Tray with Undried Soil (g)	Mass of Tray with Dried Soil (g)
B2	1308	680.8	2956.3	2589.5
B3	1149	677.4	2827.4	2444
A1	1330	685.1	3235.7	2838.7
A2	1465	693	3482.9	3007.3

Table 3.6: In-Situ Density Test Data (Part 2)

Sample	Volume (m3)	Mass of Dry Soil (kg)	Density (kg/m3)
B2	0.001308	1.909	1459.48
B3	0.001149	1.767	1537.86
A1	0.00133	2.154	1619.56
A2	0.001465	2.314	1579.52

Table 3.7: In-Situ Density Test Data (Part 3)

Sample	Water Content (kg)	Water Content (%)
B2	0.3668	0.192
B3	0.3834	0.217
A1	0.397	0.184
A2	0.4756	0.206

From the result obtained, the density of the soil in Site A is approximately 16 kN/m^3 and B is around 15 kN/m^3. On the other hand, the water content of both site is approximately 20%.

3.4 Set Up of Cyclic Triaxial System

In this section, all the procedures involving the set up of the cyclic triaxial system will be explained. This involves the set up of the loading frame, control panel, triaxial cell, sensors, data acquisition program and air pressure controller program.

3.4.1 Loading Frame

The loading frame of this cyclic triaxial system is fabricated in the university laboratory by a laboratory officer, Mr. Hwong. It consists of four long columns with a top and bottom plate. All the parts are cleaned and painted with silver paint to avoid corrosion before putting them together. To make sure that the top and bottom plates are levelled, washers are placed on the columns to adjust the height of the plate with the help of spirit level. Once everything is set, all the nuts are tighten with a spanner. After that, the air pressure cylinder is placed on top of the top plate and locked in the position.

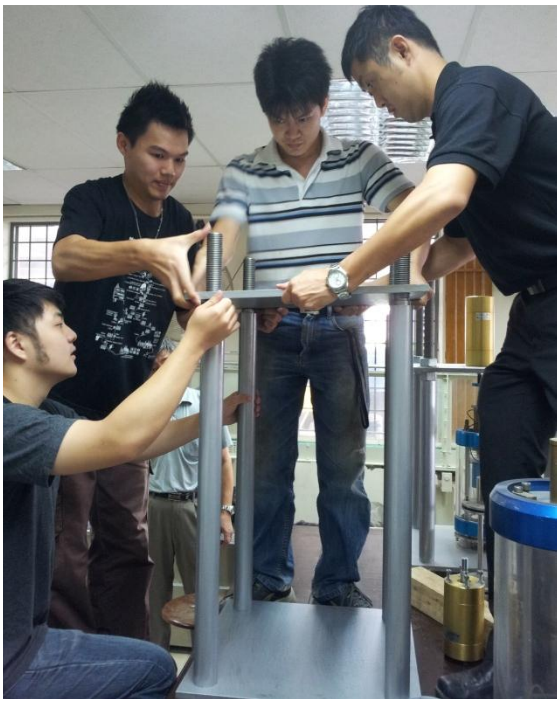

Figure 3.8: Assembling the Cyclic Triaxial Frame

3.4.2 Control Panel

The main purpose of this control panel is to placed all the controls and gauges in a same place. This control panel is made in the university laboratory. A diagram of a control panel is first drawn. The control panel is separated into four parts, namely the water supply, consolidation, pore water pressure, and axial load. The water supply section is used to supply water to the triaxial cell. Other than that, the consolidation section is used to control the consolidation pressure in the cell by adjusting the air pressure supply.

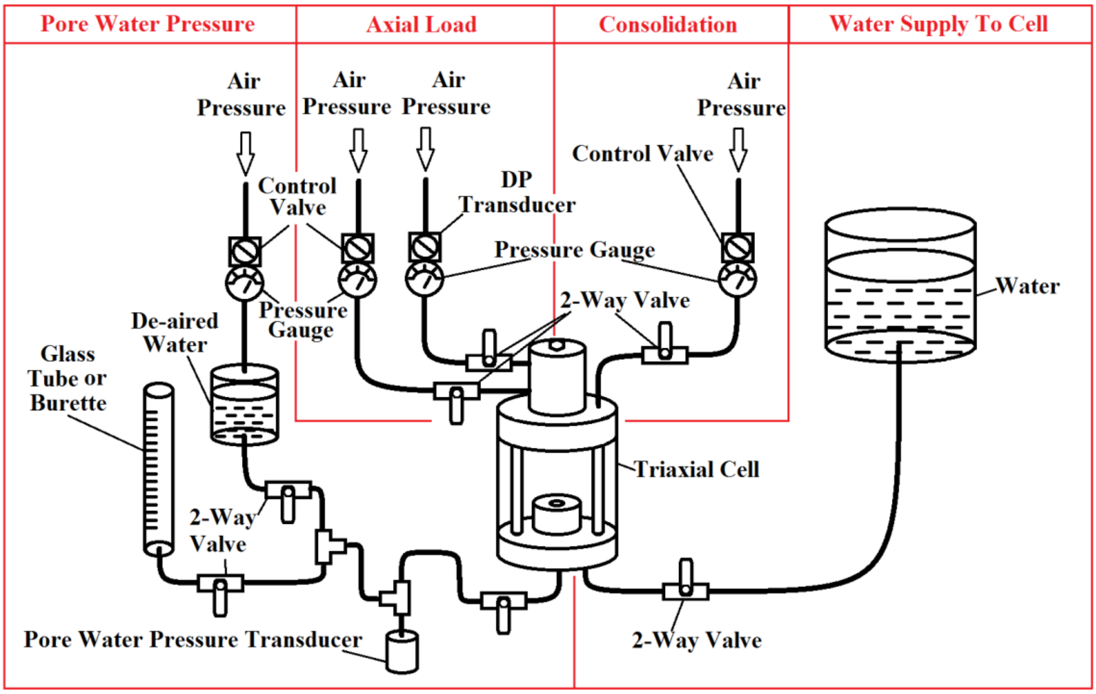

Figure 3.9: Cyclic Triaxial System Diagram

In addition, the pore water pressure section is used to supply the pressurised de-aired water to the soil sample in the cell. This can be done by supplying the air pressure into the tank filled with de-aired water before directing the water into the cell. On the other hand, there is also a glass tube with a ruler beside in this section. This is to observe the consolidation duration to make sure that the sample is completely consolidated by allowing the pore water to flow out into the glass tube.

The axial load section consists of both the manual air pressure transducer and the differential pressure transducer. This is to supply air pressure to the top and bottom of the air pressure cylinder. This will then apply load to the test specimen. A manual air pressure transducer is used at to supply the air pressure to the bottom of the cylinder manually, whereas the top cylinder is supplied by the differential pressure transducer that is controlled by an air pressure control program to generate a cyclic loading.

A PVC board is chosen to be the board of the control panel and L-shaped steel is chosen to be make frame. All the parts required like the air pressure transducer, air pressure gauge, differential pressure transducer, valves, connectors, glass tube, and ruler are placed and marked on the board. Next, the board and steel are cut into a proper length and holes are drilled on the board. After that, the board and frame are put together with nuts and bolts before securing all the parts on the board with locking straps. Locking straps are used for easy removal and assemble if the parts needed to be changed.

Once everything is in place, tubes are cut to their specific lengths and connected to the control panel. Black 6 mm tube is used to transfer air and transparent 4mm tube is used to transfer water. A transparent tube is used to make sure that there is no air bubble trapped in the tube as this will significantly affect the pore water pressure transducer reading.

Figure 3.10: Cyclic Triaxial Control Panel

In this research, the pore water pressure section is not used. Therefore, there is a modification made to it. The air pressure transducer in this section is redirected into another pressurised tank with water instead of the de-aired water tank. This water tank is then connected to the triaxial cell. The purpose of this modification is to supply water into the triaxial cell at a higher speed.

3.4.3 Triaxial Cell

This triaxial cell is imported from Kobe University in Japan by the author's research supervisor. A slight modification is made to it to suits our test by changing the valves and connectors. Some of the additional holes are sealed up to prevent any leakage. Tubes are connected to this triaxial cell after all the parts are assembled.

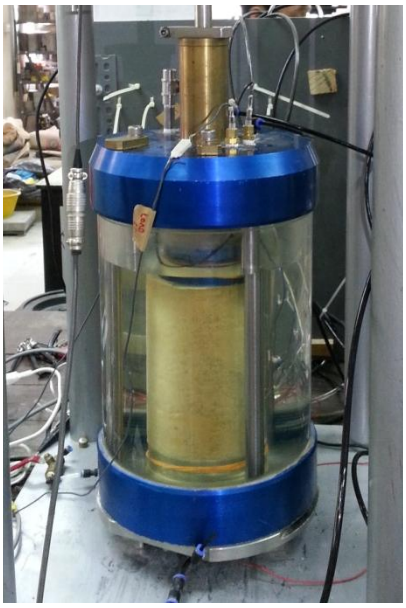

Figure 3.11: Cyclic Triaxial Cell

A special connector is fabricated to connect the triaxial cell piston and the loading piston of the air pressure cylinder. This connector is made to be adjustable on both ends and a nut is used to tighten it.

Figure 3.12: Piston Connector

3.4.4 Sensors

There is a total of three sensors used in this triaxial system. They are the Load Cell, Linear Variable Differential Transformer (LVDT), and Local Deformation Transducer (LDT). All these three sensors are explained in this section.

3.4.4.1 Load Cell

A load cell is a transducer used to measure the load in terms of millivolt. This can be done because there are four strain gauges inside the load cell to measure the strain as an electrical signal by changing the effective electrical resistance of the wire. All the strain gauges are arranged in the Wheatstone bridge configuration. The Wheatstone bridge is explained in Chapter 2. The calibration of this sensor is explained in Chapter 3.5.2.

Since the reading of load cell is in the unit of millivolt, amplifier is needed to boost up the voltage to a readable number. This Load Cell is connected to the channel 1 of the amplifier. The offset and amplification of the load cell is then adjusted carefully to the best adjustment for this research.

This load cell is placed in the triaxial cell, at the bottom of the piston. The cable is put through a hole on the triaxial cell and sealed properly with epoxy to avoid leakage when pressurising the tank.

Figure 3.13: Wire Sealed with Epoxy

3.4.4.2 LVDT

LVDT stands for Linear Variable Deformation Transformer. This sensor is used to measure the axial deformation of the sample. The reading of this LVDT is also in the unit of millivolt. Therefore, this LVDT is connected to the channel 4 of the same amplifier used by the Load Cell. The offset and amplification of this LVDT is also adjusted carefully to the best adjustment for this research. This sensor is calibrated and the procedure is explained in Chapter 3.5.4. After calibration, this LVDT is attached to the top of the frame with a magnetic indicator base.

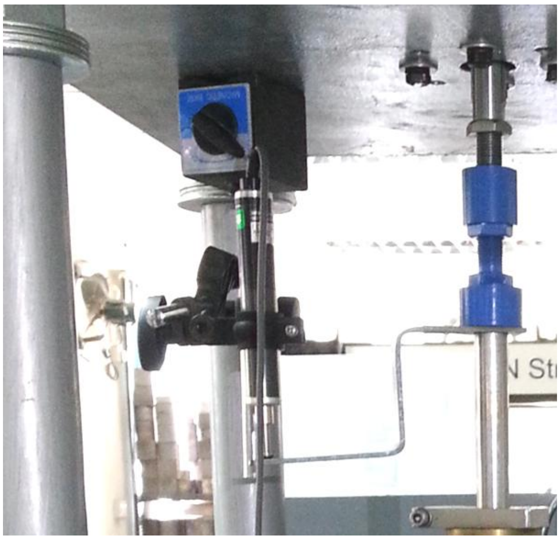

Figure 3.14: Linear Variable Deformation Transformer

3.4.4.3 LDT

LDT stands for Local Deformation Transducer. It is used to measure the deformation of the sample up to 10^{-5} strain. This LDT is made in the university laboratory. To make this sensor, four strain gauges are glued permanently to the side of a bronze strip with two strain gauge on each side. These strain gauges are then covered with a layer of flexible glue to protect them from water. The configuration of these strain gauges is using the full Wheatstone bridge.

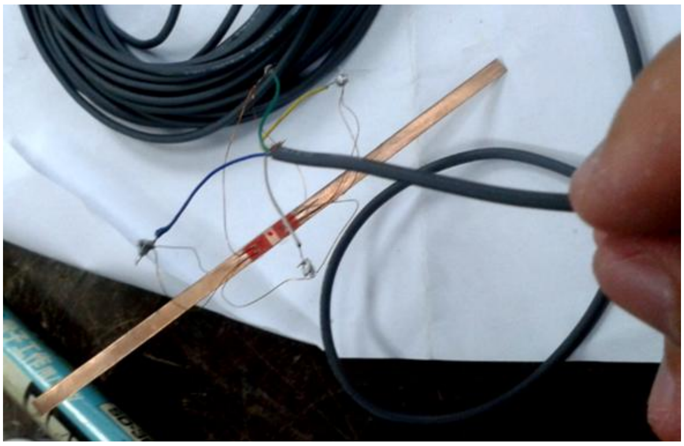

Figure 3.15: Full Bridge Connection of Local Deformation Transducer

Once all the wires are connected, they are sealed with a thin layer of glue for water proofing. After the glue is dried, this sensor is then tested and calibrated. The calibration procedure is explained in Chapter 3.5.5.This sensor is then attached to the side of the soil sample before testing with two clips glued to the membrane.

The voltage received from this LDT is in mV. Therefore, an amplifier is needed as well. Since this transducer is extremely sensitive, a better amplifier is used. The amplifier is then adjusted to the best amplification the author can obtain before doing any calibration. The calibration of this sensor will be explained in Chapter 3.5.5.

3.4.5 Data Acquisition with LabVIEW

LabVIEW is a graphical programming software that uses to create applications to communicate with hardware such as data acquisition device. This software enable user to create a user interface to operate the specific instruments. LabVIEW programs are called virtual instruments, also known as VIs.

In this research, LabVIEW is required to acquire data from the sensors because that the cyclic loading is continuous and the data acquisition speed must be fast enough to produce a better result. This precise and fast data acquisition process is beyond what human can do manually. Therefore, LabVIEW is needed for this purpose. The hardware used to acquire data is called USB-6210. This device requires LabVIEW 2009 to run.

A program named Data Acquisition is created with LabVIEW by the author. The author used the function of While Loop, For Loop, Time Delay, DAQmx Read (Analog 1D Wfm NChan 1Samp), Split Signals, Waveform Chart, Convert from Dynamic Data, Property Node, Write to Measurement File, Divide, Multiply, and

Add Array Elements are used. The arrangement of all these functions in Block Diagram is shown in the figures below.

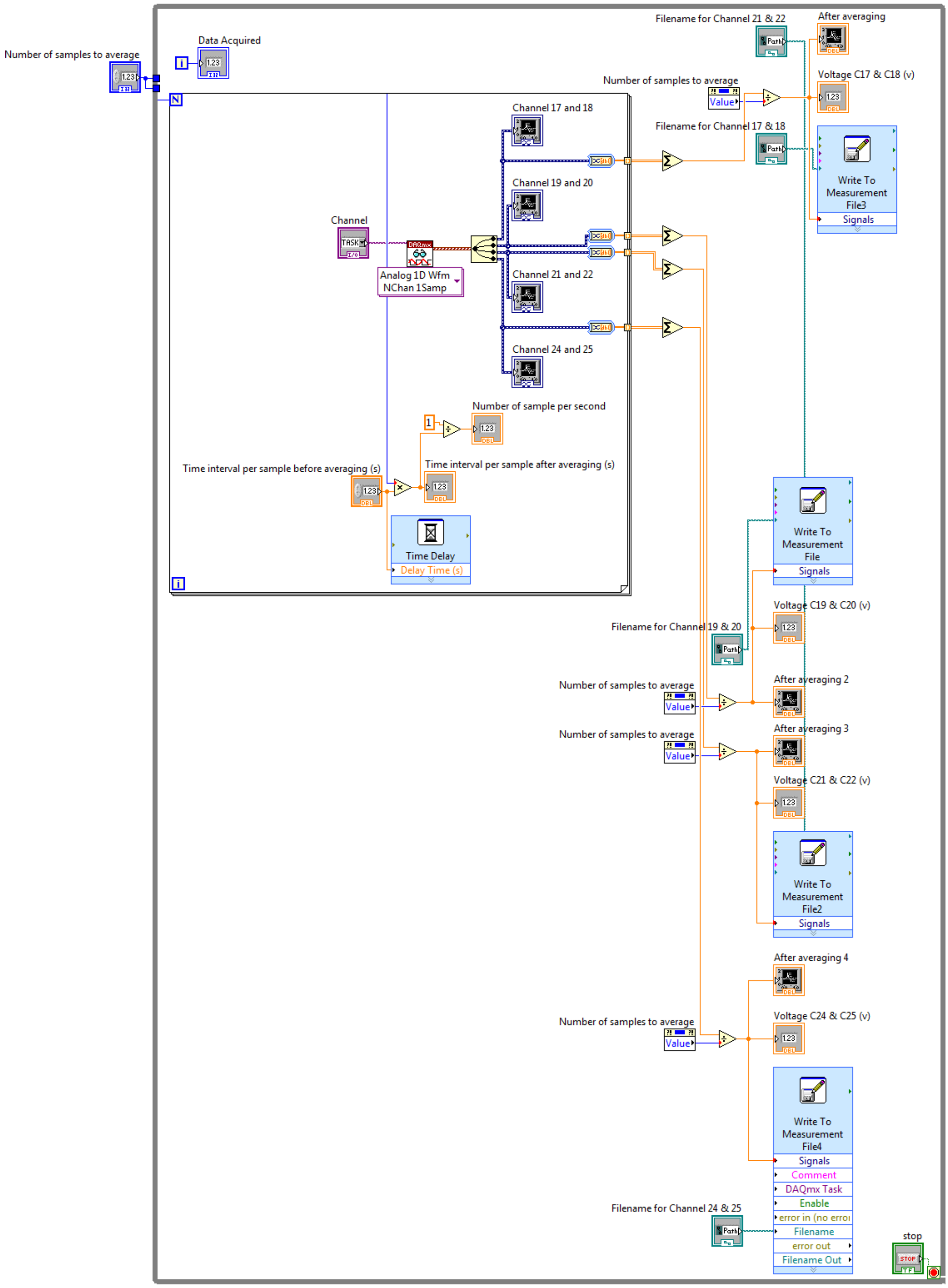

Figure 3.16: Block Diagram of Data Acquisition Program

In addition, the Front Panel is the place where all the controls are shown. This Front Panel is used by user to control this program while using it. The Front Panel is shown in the figures below.

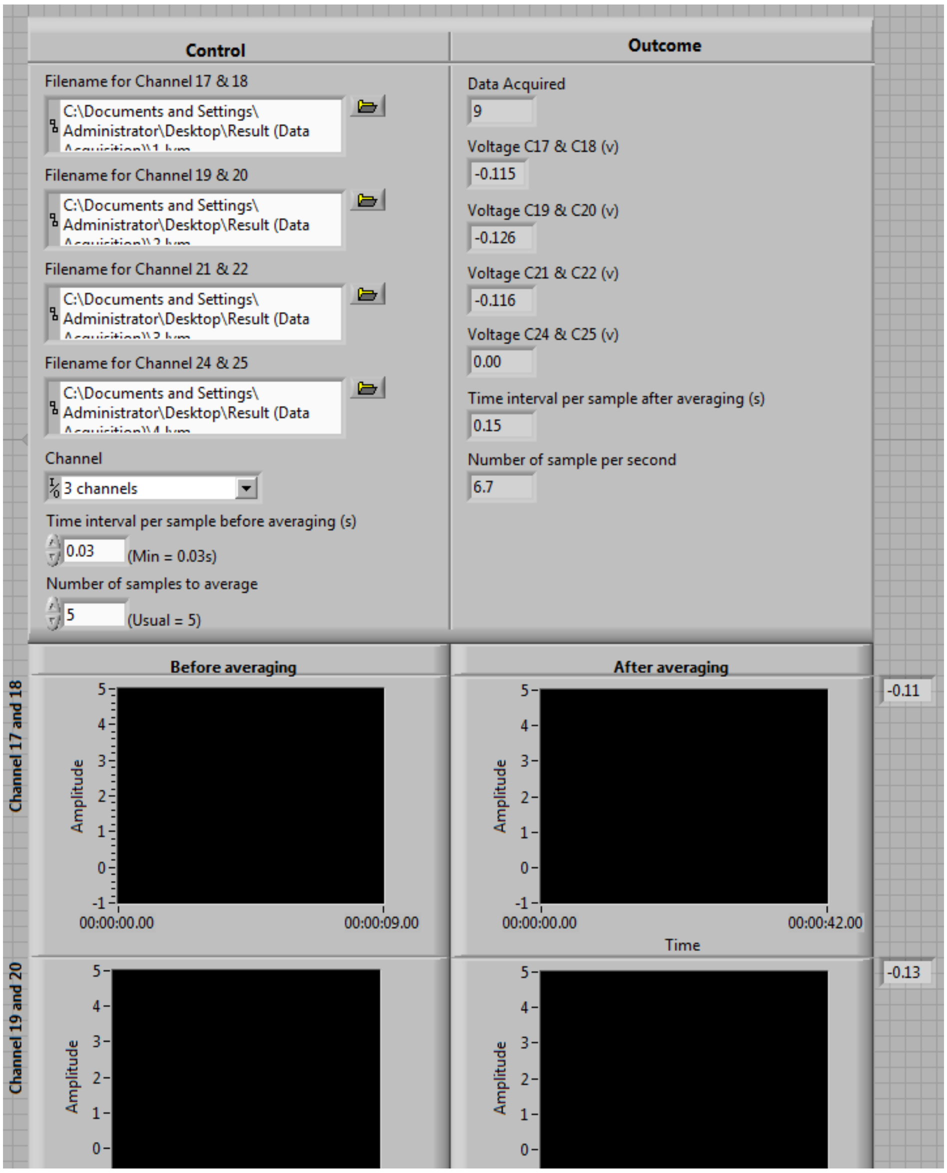

Figure 3.17: Front Panel of Data Acquisition Program

This program is able to acquire the data at the speed of 0.03 seconds per sample. Since there are some noises generated by some of the electronic devices and some external factors, this program also has a function to average the data acquired by simply changing the number of data to be averaged. By default, the number of data to be averaged is 5. All the data will be stored in the computer in the file typed by the user. Channel 17 & 18 is set by the author for Load Cell and Channel 19 & 20 is for LVDT, whereas Channel 21 & 22 is for LDT. Channel 17, 19 and 21 are the positive connection, whereas Channel 18, 20 and 22 are the negative connections.

The file saved is in the format of tdms. An Microsoft Excel plugin called tdm_excel_add-in_2012.exe is needed to be installed in the computer in order to read this file with Microsoft Excel. This plugin is included in the CD attached to this report. The result will be shown in sheet two instead of the first sheet in Microsoft Excel.

3.4.6 Controlling DP Transducer with LabVIEW

A DP Transducer is also called a Differential Pressure Transducer. This transducer is used to control the air pressure supply to the air pressure cylinder. LabVIEW is required to generate a sine wave to the DP Transducer in order to produce a smooth cyclic loading. DAQCard-1200 device is used for this purpose. This device can only runs in LabVIEW 6.1 on Windows XP. The connector pin of this device is shown below.

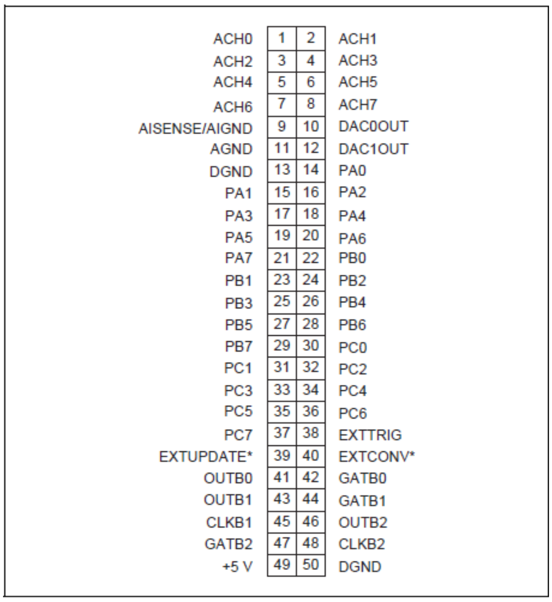

Figure 3.18: DAQCard-1200 I/O Connector Pin Assignments (National Instruments, 1999)

The channels the author used are Channel 10 and Channel 11. Channel 10 is the positive connection, whereas the Channel 11 is the negative connection.

A program is created by the author that named Air Pressure Controller. This program uses the function of While Loop, For Loop, Case Structure, Sine, To Double Precision Float, Waveform Chart, AO Update Channel, Wait Until Next ms Multiple, Wait (ms), Property Node, Not, Divide, Multiply, Add and Equal for this program. The arrangement in the Block Diagram is shown in the figures below.

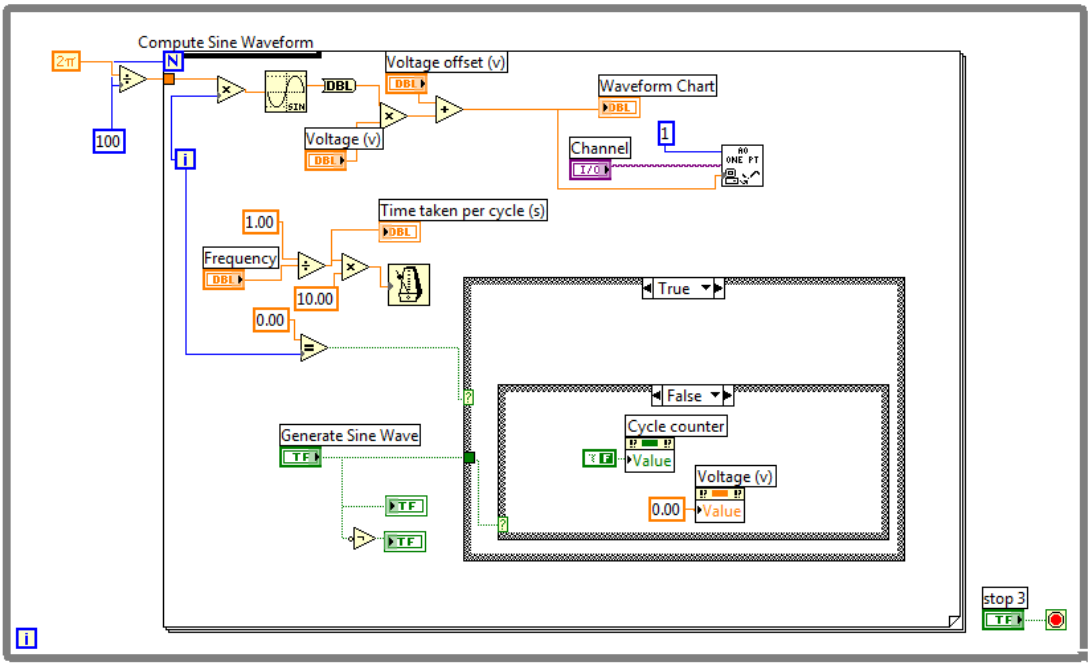

Figure 3.19: Generate Sine Wave

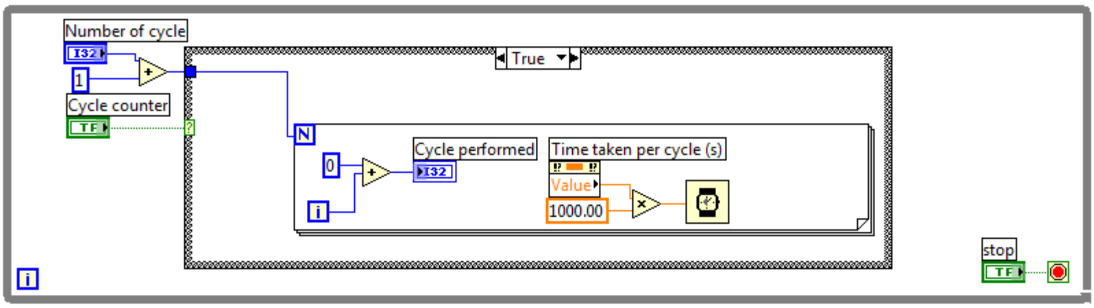

Figure 3.20: Cycle Counter

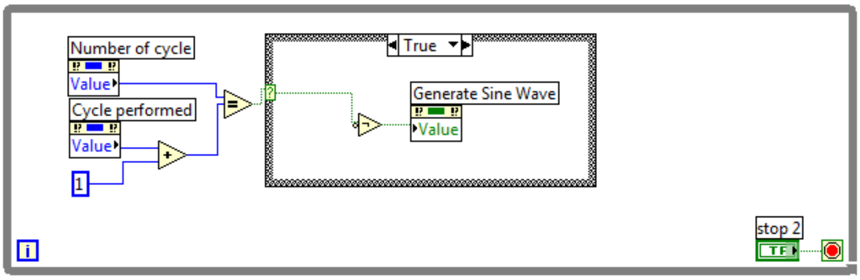

Figure 3.21: Generate Sine Wave Start Button

The Front Panel will the one with all the controls will appear. All these controls are used to control the DP Transducer. This Front Panel is shown in the below.

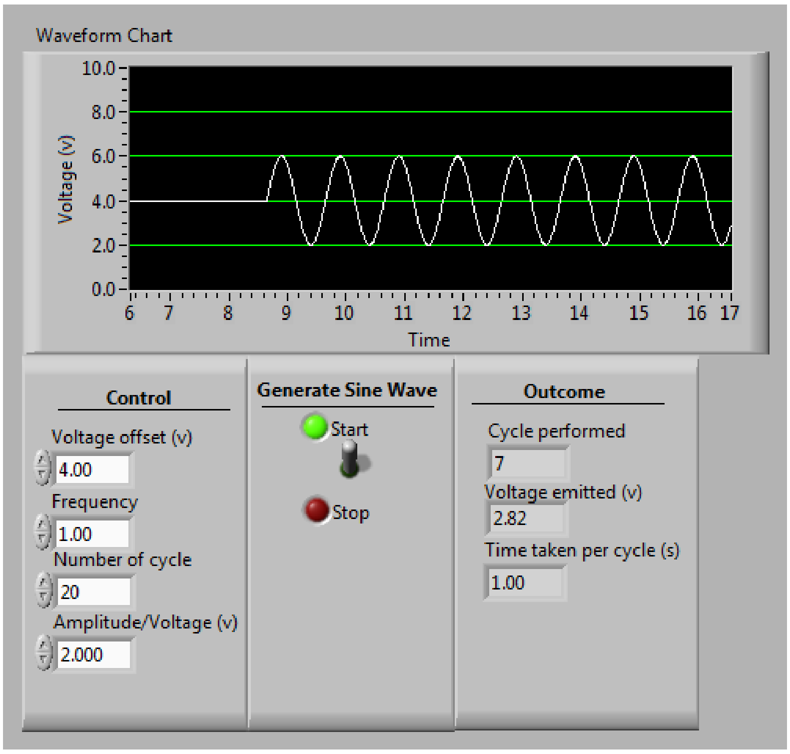

Figure 3.22: Air Pressure Controller Front Panel

3.5 Calibration

The purpose of calibration is to enable us to convert the voltage received from the sensors to the unit that the author wanted, such as kilogram, bar and millimetre. In this section, the calibration of Differential Pressure Transducer, Load Cell, axial load, Linear Variable Deformation Transformer (LVDT), and Local Deformation Transducer (LDT) is explained in this section of this chapter.

3.5.1 DP Transducer Calibration

This DP Transducer, also known as Differential Pressure Transducer, is calibrated by connecting to the DAQCard-1200 that is plugged in to the laptop. Data Acquisition program is used to instruct the DAQCard-1200 to emit voltage to the Differential Pressure Transducer.

Voltage is increased slowly until the air pressure gauge showed or 1 bar. Then the voltage value is recorded. After that, the voltage is increased again until the gauge showed 1.5 bar and the voltage is recorded. This step is repeated a few times at the interval of 0.5 bar until it reached 5 bar. Next, the voltage is reduced at the interval of 0.5 bar until it reached 1 bar again. Once all the data is collected, a graph of Voltage Supply vs Air Pressure is plotted and the gradient of the graph is obtained. The calibration data is shown in Appendix A.

After calibration, the relationship of voltage supply and air pressure is shown in the equation below:

$$v = 1.231621a \tag{3.1}$$

where

v = voltage supply, V

a = air pressure, bar

3.5.2 Load Cell Calibration

Before calibrating the Load Cell, the limit of this Load Cell should be found first. This can be done by first placing the triaxial cell on the floor with the Load Cell attached to the bottom of the piston. A steel cylinder is placed at the place where the soil sample will be placed to act as a support so that the piston will not go all the way down. A few steel plates are weighted on a weighing scale and recorded down. Then the Load Cell is connected to a data logger and the data logger is set to Simple Measure to measure the strain of the Load Cell.

The initial strain is recorded before placing any load on the piston. Next, the first load is placed on the piston and the mass of the load and the strain shown in the data logger is recorded. This step is repeated a few more times until the mass reached around 15 kg. Then, the steel plate is reduced one by one and the data is recorded for every removal of the steel plate. After that, a graph of mass vs strain is plotted and the equation is obtained from the graph. This equation is shown below:

$$m = (-1.659346 \times 10^{-1})s - (8.265608 \times 10^{-2}) \qquad (3.2)$$

where
m = mass, kg
s = strain, με

Since the maximum strain it can go is 3000 με, this value is substituted into equation 3.2 and obtained the maximum mass, which is 497.72 kg. The data for this calibration is shown in Appendix B.

After knowing the Load Cell limit, the Load Cell can be calibrated by connecting the Load Cell to an amplifier. The amplifier is then connected to the USB-6210 device. After that, the USB-6210 device is plugged in to the laptop. Data Acquisition program is used to acquire the reading of the Load Cell in the unit of millivolt.

The initial reading of the voltage emitted by the Load Cell is recorded. Then, the first steel plate is placed on the piston. After that, the mass of the steel plate and the voltage shown in the Data Acquisition program is recorded. This step is repeated a few more times with more load placed on the piston until it reached around 80 kg. Then the step is repeated again by reducing the steel plate one by one. Once the data is collected, a graph of voltage vs mass is plotted and the gradient is obtained from the formula of the graph. This calibration data is shown in Appendix C. With the use of the gradient obtained from the graph, the relationship of voltage and mass is shown below:

$$v = (-3.525791 \times 10^{-5})m \tag{3.3}$$

where
v = voltage received from Load Cell, V
m = mass, g

3.5.3 Axial Load Calibration

In order to obtain the relationship of the air pressure supplied to the air pressure cylinder and the voltage received from the Load Cell, another calibration is done by first placing the triaxial cell on the triaxial frame and connected the piston of the cell to the piston of the air pressure cylinder. A steel cylinder is placed in the location where the soil sample supposed to be placed to act as a support. Then, all the necessary devices and parts are connected. Next, the voltage emitted by the DAQCard is increased to increase the air pressure at the interval of 0.5 bar until it reached 2.5 bar. At each interval, the air pressure and the voltage from the Load Cell is recorded. This step is repeated again with the decrease of the air pressure at the same interval.

After obtaining the data, all the voltage obtained from the Load Cell is converted to mass in gram by using equation 3.3. Then the unit is changed from gram to kilogram by dividing by another one thousand. A graph of mass of load vs air pressure is plotted and the gradient is obtained. This calibration data is shown in Appendix D and the relationship of air pressure and mass is shown below:

$$m = 46.78143a \tag{3.4}$$

where
m = mass, kg
a = air pressure, bar

However, the relationship of voltage supplied by DAQCard-1200 and the load applied to the soil sample must be found. With this relationship, the load can be controlled by the DAQCard-1200 by simply converting the voltage to kilogram or vice versa. This relationship can be found by combining equation 3.1 and 3.4 to form a new equation below:

$$v = \left(\frac{m}{46.78143}\right) \times 1.231621 \tag{3.5}$$

where
v = voltage supplied by DAQCard-1200, V
m = mass of load acting on soil sample, kg

3.5.4 LVDT Calibration

The Linear Variable Deformation Transducer is calibrated by using a soil sample extruder. This can be done by clamping the LVDT to one end of the extruder and a dail gauge is clamped on the other end. By rotating the handle of the extruder, the metal bar will move horizontally. This will eventually push or release the LVDT and the dail gauge on the other end will be affected as well. This set up is shown in the below.

Figure 3.23: Calibration of LVDT

The LVDT is connected to the amplifier and the amplifier is connected to the USB-6210 device that is plugged to the laptop. Once everything is set up, the LVDT is pushed in until it reached the third line from the tip of the LVDT as shown in the below. This is to set the initial position of the LVDT. After that, the initial voltage and the dail gauge reading is recorded.

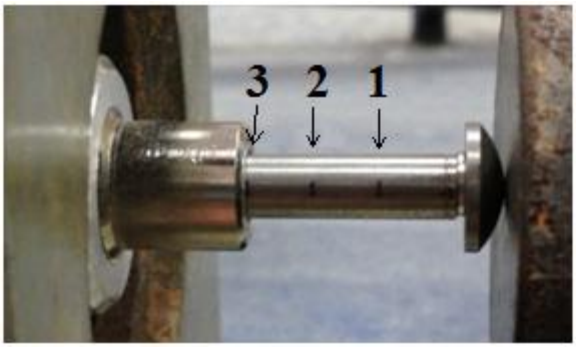

Figure 3.24: Initial Position of LVDT

Next, the extruder is rotated anti-clockwise slowly until the dial gauge reading increase by 25 division or 0.25 mm. Then, the voltage reading and the dail gauge reading is recorded. This step is repeated at the interval of 25 division until 600 division or 6 mm. After that, the extruder is rotated clockwise and the procedure is repeated again. A graph of voltage vs dail gauge reading is plotted and the data is shown in Appendix E. From the gradient of the graph plotted, the relationship between voltage and deformation is shown below:

$$v = (6.531692 \times 10^{-3})d \tag{3.6}$$

where
v = voltage received from LVDT, V
d = deformation or displacement, 0.01 mm

3.5.5 LDT Calibration

The Local Deformation Transducer is calibrated by using the same extruder used to calibrate the LVDT. A dial gauge is clamped to once end of the extruder, whereas the other end is used to place the LDT. A piece of cardboard with a small cut in the middle is taped on the extruder to hold the LDT by slotting the LDT into the cut. The set up is shown in the below.

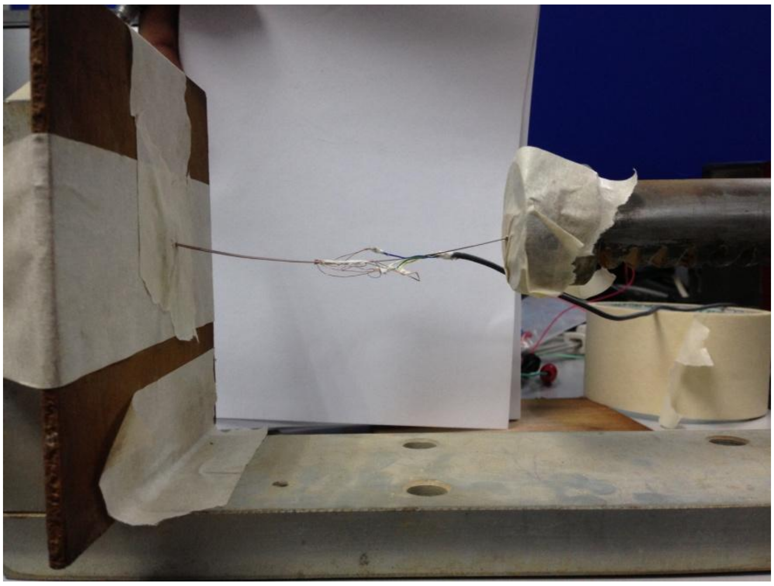

Figure 3.25: Initial Position of LDT

Firstly, the initial position of the LDT is set by connecting the LDT to a data logger that is set to Simple Measure to measure the strain. The initial strain and the dial gauge reading is recorded. After that, the extruder is rotated anti-clockwise to compress the LDT for every 15 division of the dial gauge reading until 135 division or 1.35 mm. For each interval, the reading of the dial gauge and strain from the data logger is recorded. A graph of strain vs deformation is plotted. This data is shown in Appendix F.

The graph plotted is in the form of a curve instead of a linear line. This shows that the response of this LDT will reduce as the deformation go higher. Therefore, the initial position is set to only 1 mm. The equation of the graph is shown below:

$$s = (-1.022391 \times 10^{-1})d^2 + 38.60631d - (6.201182 \times 10^2) \tag{3.7}$$

where
s = strain, με
d = deformation, 0.01mm

From the equation above, the strain of the initial position, which is 1 mm deformation is calculated to be 2218 με. To calibrate the LDT, it is first set to this initial position by connecting it to data logger and deform until it reached 2218 με. After that, the LDT is connected to the amplifier and the amplifier is connected to the laptop with the Data Acquisition program.

The extruder is then rotated at the interval of 5 division from the dial gauge reading until it reached 150 division or 1.50 mm. At every interval, the dial gauge reading and the voltage is recorded. The test is repeated from the other direction. All the data obtained is shown in Appendix G. A graph of strain vs voltage is plotted and the equation is shown below:

$$d = (1.178548 \times 10^{-1})v^2 - 14.32758v - 7.566959 \tag{3.8}$$

where
d = deformation of LDT, 0.01 mm

v = voltage received from LDT, V

3.6 Testing Procedure

In this section, the procedure to perform a test on the soil specimen with the cyclic triaxial system is explained. This includes the test specimen preparation, the mounting of the specimen, the consolidation procedure, and the cyclic loading process.

3.6.1 Test Specimen Preparation

First, the mould is then cleaned and coated with a layer of oil to allow the sample to be removed from the mould easily. Then mould is clamped with G-clamps. Specially made wood blocks should be placed in between the G-clamps and the mould to protect the mould from damaging and also to prevent sliding. This mould is then placed under the Hydraulic Press Machine with a steel plate at the bottom.

To prepare a specimen, the amount of soil and water is calculated based on the density of 16 kN/m^3 and water content of 20%. This calculation is in Appendix H. Then, they are mixed together with the water poured in slowly until they are evenly mixed. This has to be done in a place without any wind to prevent excessive loss of water from the soil.

After mixing, the soil is separated into four parts. A custom made piston is measured and marked to four evenly distributed layer. One part of the soil is then placed into the mould first and the custom made piston is placed into the mould. Then the compaction process is started until it reached the first marked line. After that, the piston is removed and the surface of the compacted soil is scratched to give a better bonding with the next layer. This step is repeated three more times for the next three layer.

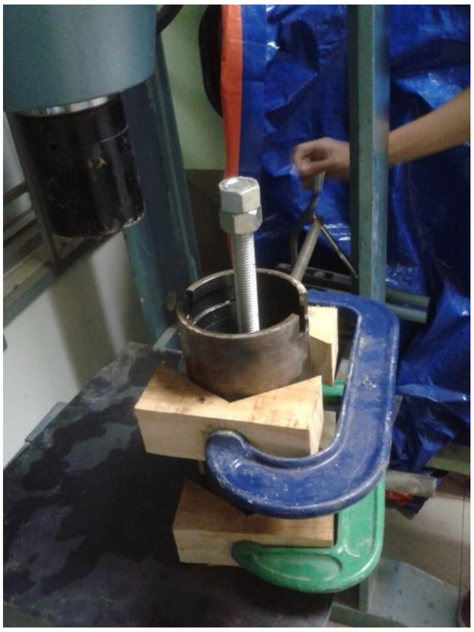

Figure 3.26: Compacting the Soil

After compaction, the mould is removed carefully and the dimension of the sample is measured with a calliper. Plus, the weight of the sample is also taken. This soil sample is then wrapped up with plastic sheet to prevent any loss of water content while preparing the other necessary things for testing.

Figure 3.27: Compacted Soil Sample

3.6.2 Specimen Mounting Procedure

First, a clean membrane is placed into the membrane stretcher. Then, the membrane is folded over at the top and bottom of the membrane stretcher. After that, suction is introduced to the tube of the membrane stretcher to expand the membrane in the membrane stretcher. Once the membrane is fully expanded inside, the tube is clipped to maintain the pressure inside the membrane stretcher.

Figure 3.28: Membrane Folded Over the Membrane Stretcher

After that, the soil sample is placed inside the membrane and the clip on the tube of the membrane stretcher is removed to allow the membrane to wrap around the soil. Then, the soil sample is removed from the membrane stretcher along with the membrane. Next, the top and bottom of the excess membrane is folded over, exposing the top and bottom surface of the soil.

Filter paper is then placed on the top and bottom surface of the soil before placing it to the triaxial cell. Silicone grease is applied on around the side of the loading cap and the bottom cap. Rubber bands are placed at the top of the loading cap. Then, the membrane is folded over the loading cap and bottom cap before lowering the rubber bands to the loading cap and bottom cap to seal the membrane.

Figure 3.29: Soil Sample with Filter Paper

After that, the LDT cable is connected to the amplifier, USB-6210 and laptop. The bottom LDT clip is glued to the side of the membrane with a fast drying glue. Then, the Data Acquisition program is started. Once the program is receiving signal from the LDT, the LDT is placed on the glued bottom clip and adjusted to around -6 to -7 V, which is the 1 mm initial position of the LDT, by using a tweezer to grip on the top clip that is placed on the top of the LDT. Glue is applied immediately after the LDT reading is around -6 to -7 V. The tweezer is removed after the glue is dried.

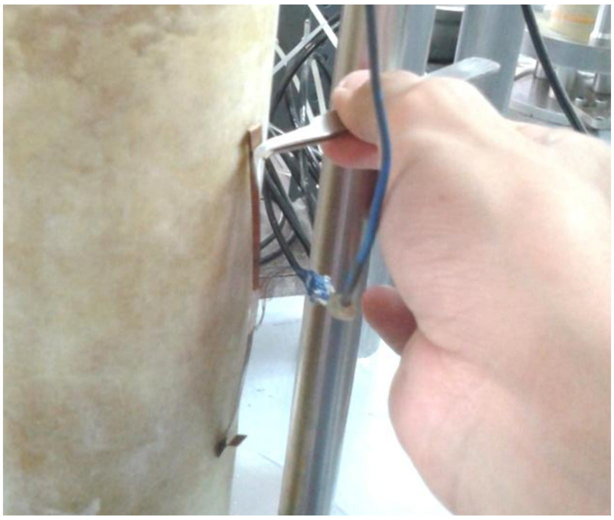

Figure 3.30: Attaching the LDT to the Membrane

Next, the LDT cable is detached from the triaxial cell. Grease is applied on the top and bottom O-ring before placing the triaxial cell cover and locking it. Then, the cell is pushed to the centre position and all the three sensors, consolidation tube and water supply tube are connected.

3.6.3 Consolidation

All the valves on water tank, control panel and triaxial cell are closed except the pore water drainage valve. Then, the water supply valve and water supply air pressure valve is opened. The air pressure is then increased up to 1 bar to allow the water to enter the tank. Once the water reached the half of the loading cap, the water supply valve and the water supply air pressure valve is closed. Then, the air pressure is reduced to zero and the release valve of the water tank is opened.

The Voltage Offset is set to zero before running the Air Pressure Controller program. Once the Air Pressure Controller program is started, it can only be turned off after every test is completed to avoid any changes to the top air pressure. After that, the bottom air pressure valve and the pressure is adjusted to 2 bar. Next, the top air pressure valve is opened and the voltage supply from the DAQCard-1200 is adjusted to 2 bar slowly, which is 4.10 V, by increasing the Voltage Offset to make the piston fall about 2.5 cm. To prevent the piston from coming down too fast, the bottom air pressure is increased and decreased manually.

Once the piston reached 2.5 cm and stopped moving, the specially made connector is connected to both the piston of the air pressure cylinder and the piston of the triaxial cell. Then, the LVDT is adjusted to the initial position, which is the third line counting from the tip of the LVDT. The initial reading of the Load Cell, LDT and LVDT is recorded.

The consolidation air pressure is increased 1 bar. After that, the consolidation valve is opened and the stopwatch is started at the same time. The Load Cell voltage will change once the consolidation is started. The top air pressure is adjusted immediately with the Air Pressure Controller program until the Load Cell voltage is adjusted back to the inital voltage recorded earlier.

The reading of Load Cell, LDT and LVDT is recorded at the interval of 15s, 30 s, 60 s, 90 s, 120 s, 180 s, 240 s, 360 s, 480 s, 600 s, 900 s, 1200 s, 1500 s, 1800 s, 2400 s, 3000 s, 3600 s, 4200 s, 4800 s, 5400 s, 6000 s, 6600 s, 7200 s, and 7800 s. Once all the data is collected, a graph of deformation vs logarithmic scaled time is plotted. When the deformation is becoming near to a constant value after a long duration, the consolidation process is assumed to be completed. This consolidation data is shown in Appendix I.

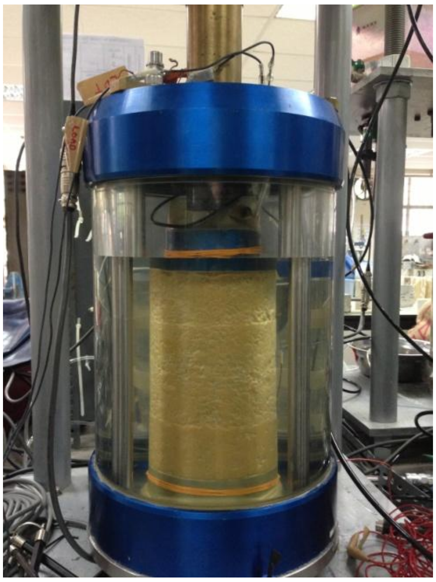

Figure 3.31: Consolidation Process

3.6.4 Cyclic Loading

The stress ratio, which is a ratio between the half of deviator stress and the confining pressure, applied in this research is 0.01, 0.02, 0.05, 0.07, 0.10, 0.12, 0.15, 0.20, 0.25, 0.30, and 0.35. For each stress ratio, five different frequencies are tested. They are 0.1 Hz, 0.2 Hz, 0.5 Hz, 0.8 Hz, and 1 Hz. To start the cyclic loading, the Frequency, Amplitude and Number of Cycle is set based on the calculation in Appendix M, starting with the lowest load and lowest frequency. The file name of Channel 17 & 18, Channel 19 & 20, and Channel 21 & 22 is changed.

Then, the Data Acquisition program is started and the Generate Sine Wave button is pressed. The time shown on the Data Acquisition program is recorded immediately after the Generate Sine Wave button is pressed. The time is recorded again after all the cycles are generated. After that, the Data Acquisition program is stopped. This whole process is repeated a few more times for the next frequency starting from low to high frequency by changing the Frequency in the Air Pressure Controller program. Next, a few more sets of this whole process is repeated again for the next higher load starting by changing the Amplitude value.

After the last test is completed, the water supply valve is opened to allow the water to flow back to the tank. Once all the water is flowed back to the tank, the water supply valve is closed. Next, the consolidation air pressure is reduced to zero and the consolidation valve is closed. After that, the triaxial cell air pressure release valve is opened. The connector is then removed from the pistons and the top air pressure is reduced to zero by changing the Voltage Offset to zero. Then, the bottom air pressure is also reduced to zero and closed both the top and bottom air pressure valve.

Everything is then removed from the triaxial cell and the soil sample is taken out. The dimension of the soil sample is measured again at a few locations. After that, a small amount of the soil sample is taken from the middle of the sample for water content testing.

3.7 Data Analysis

The dynamic properties that the author have to obtained from this research is the shear modulus, *G*, and the damping ratio, D. To obtain these two properties, several steps has to be done.

Firstly, graph of the voltage vs time is plotted from the Load Cell of every test. Then the first and last point of the 20 cycles is recorded. Plus, the beginning point of the twentieth cycle is also recorded. After that, the values outside the range of the first and last point is removed. Then, all the data is placed in the same Excel file.

After that, the voltage received from the LVDT and LDT is converted to deformation by using equation 3.6 and 3.8. Then it is divided by 100 to change the unit to mm from 0.01 mm. This value is then divided by the height of the sample to obtain the axial strain.

Next, the initial area of the specimen before the cyclic loading is calculated by assuming that the axial strain is equal to the volumetric strain during consolidation. The area can be calculated with the formula below.

$$A_1 = \frac{A_0(1-3\epsilon_a)}{1-\epsilon_a} \tag{3.9}$$

where
A_1 = area after consolidation, m^2
A_0 = area before consolidation, m^2
ϵ_a = axial Strain

To obtain the axial strain, the voltage difference is calculated before converting to deformation with equation 3.8. Then the deformation is divided by another 100 to change the unit to mm instead of 0.01 mm. After that, it is divided by the initial height of the sample to obtain the strain.

However, to calculate the new area after every single cyclic loading is completed, another different formula is needed. This formula can be derived by assuming that the volume of the soil sample remain the same after each cyclic loading test is completed. The formula is shown below.

$$A_1 = \frac{A_0}{1-\epsilon_a} \tag{3.10}$$

where

A_1 = area after cyclic loading, m^2

A_0 = area before cyclic loading, m^2

ϵ_a = axial strain based on the LDT

The next step is to convert the Load Cell voltage to stress ratio. This is done by using equation 3.3 to convert voltage to mass in gram. Then the unit gram is converted to kg by dividing with 1000. This value is then divided by the area, A_1 to convert kg to kg/m^2. Next, it is divided again by 100 to convert kg/m^2 to kN/m^2 or kPa. This is then divided again by 2 and 100 kPa, where 100 kPa is the consolidation pressure, to convert kPa to stress ratio. The formula to convert the deviatoric stress (kPa) to stress ratio is shown below.

$$SR = \frac{\left(\sigma_d/_2\right)}{\sigma_c} \tag{3.11}$$

where

SR = stress ratio

σ_d = deviatoric stress, kPa

σ_c = consolidation pressure, kPa

After that, graph of stress ratio vs axial strain is plotted for every set of data. Two different graphs are plotted with the axial strain based on LDT and LVDT for comparison purpose. After that, the twentieth cycle graph is also plotted for those with loop appeared on the graph.

In addition, the young modulus for those graph without loop is obtained by first drawing a best fit line on the graph and then the gradient is multiplied with 200, then this will be the young modulus. To obtain the young modulus from those graph with loop, the most left and right point is obtained from the graph and the gradient is calculated. After that, the gradient is also multiplied with 200. This is explained in the equation below after combining with equation 3.11.

$$E = \frac{(\sigma_2 - \sigma_1)}{(\epsilon_2 - \epsilon_1)} = \frac{(SR_2 - SR_1)}{(\epsilon_2 - \epsilon_1)} \times 200 = \text{gradient of graph } \times 200 \tag{3.12}$$

where

E=young modulus, kPa

σ_2 = stress of second point, kPa

σ_1 = stress of first point, kPa

SR_2 = stress ratio of second point

SR_1 = stress ratio of first point

ϵ_2 = axial strain of second point

ϵ_1 = axial strain of first point

After that, the young modulus is converted to shear modulus with the formula below.

$$G = \frac{E}{2(1+\mu)} \tag{3.13}$$

where

G = shear modulus, kPa

E = young modulus, kPa

μ = poisson ratio, 0.5

To calculate the damping ratio, area of the twentieth cycle loop has to be calculated first. This area can be calculated using the trapezoidal rule by assuming that all the area below the graph is a combination of many trapezium. After that, the area of the triangle shown as the shaded region in the below is also obtained.

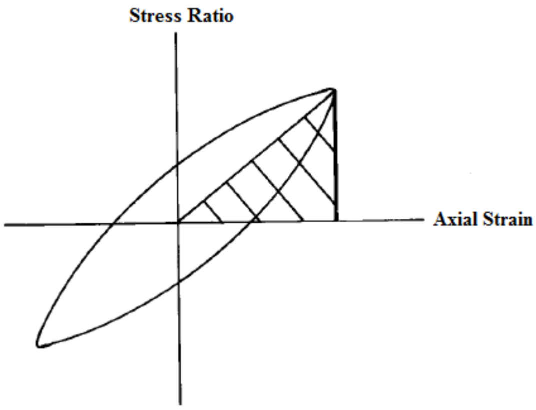

Figure 3.32: Area of Triangle

After obtaining both areas, the damping ratio can be calculated with the formula below.

$$D = \frac{A_{loop}}{4\pi A_{triangle}} \times 100 \qquad (3.14)$$

where
D = damping ratio, %
A_{loop} = area of the hysterical loop
$A_{triangle}$ = area of triangle

Next, the axial strain is converted to shear strain with the formula below, assuming that the volume remained unchange.

$$\gamma = 1.5 \in_a \qquad (3.15)$$

where
γ = shear strain
ϵ_a = axial strain

Once all the data is obtained, a graph of shear modulus vs shear strain, damping ratio vs shear strain, shear modulus vs frequency, damping ratio vs frequency, shear modulus vs stress ratio, and damping ratio vs stress ratio are plotted. All these data is in the CD attached to this report.

CHAPTER 4

RESULTS AND DISCUSSION

4.1 Introduction

This chapter presents the results of cyclic triaxial tests and the discussion about the result and this research. Also, this chapter explains the problems encountered during this research and the ways to solve them.

4.2 Dynamic Properties

The shear modulus and damping ratio obtained from this research are shown on the two tables below.

Table 4.1: Shear Modulus

Stress ratio	Frequency	Shear Modulus, G (kPa)	Shear Strain, γ (%)
0.01	0.10	1.194897E+05	1.102445E-03
	0.20	1.233955E+05	9.993000E-04
	0.50	1.320455E+05	8.327610E-04
	0.80	1.023557E+05	3.648300E-04
	1.00	9.447747E+04	4.203531E-04
0.02	0.10	1.293557E+05	2.347554E-03
	0.20	1.311629E+05	1.959023E-03
	0.50	1.342574E+05	1.261086E-03
0.05	0.10	1.082608E+05	5.420220E-03

	0.20	9.283173E+04	3.405005E-03
	0.50	9.790333E+04	2.976465E-03
0.07	0.10	1.115869E+05	7.532295E-03
	0.20	1.112614E+05	6.755064E-03
	0.50	1.157525E+05	5.136098E-03
	0.80	1.150913E+05	3.929355E-03
0.1	0.10	1.059014E+05	1.311374E-02
	0.20	1.053769E+05	1.222518E-02
	0.80	1.084486E+05	8.756655E-03
	1.00	1.132985E+05	7.573589E-03
0.12	0.10	94542.78221	1.654143E-02
	0.20	95250.37252	1.595424E-02
	0.50	101051.5369	1.423907E-02
	0.80	104156.8531	1.209485E-02
	1.00	102227.0523	9.815295E-03
0.15	0.10	94797.92818	2.267891E-02
	0.20	91225.62553	2.236455E-02
	0.50	95758.90508	2.037936E-02
	0.80	94838.9569	1.646951E-02
	1.00	93860.56143	1.479200E-02
0.2	0.10	57989.6013	4.136535E-02
	0.20	57140.37621	4.306532E-02
	0.50	66622.63371	3.985616E-02
	0.80	61089.1204	3.622640E-02
	1.00	56992.06251	3.087420E-02
0.25	0.10	42536.58315	7.377873E-02
	0.20	40287.19109	7.532919E-02
	0.50	43308.57443	6.727035E-02
	0.80	41332.39791	5.521947E-02
	1.00	42661.84062	4.462950E-02
0.3	0.20	22294.30213	1.568466E-01
	0.50	22482.57549	1.433911E-01
	0.80	26981.12635	1.072913E-01
	1.00	27006.44581	8.500074E-02

Table 4.2: Damping Ratio

Stress ratio	Frequency	Damping Ratio (%)	Shear Strain, γ (%)
0.12	0.10	6.459909417	1.654143E-02
	0.20	7.99956743	1.595424E-02
	0.50	8.11330736	1.423907E-02
	0.80	8.959754385	1.209485E-02
	1.00	8.126266921	9.815295E-03
0.15	0.10	8.397462409	2.267891E-02
	0.20	9.855325706	2.236455E-02
	0.50	10.13944862	2.037936E-02
	0.80	11.86756565	1.646951E-02
	1.00	8.967820876	1.479200E-02
0.2	0.10	4.173970619	4.136535E-02
	0.20	18.37682569	4.306532E-02
	0.50	14.96307836	3.985616E-02
	0.80	16.30639587	3.622640E-02
	1.00	19.79063932	3.087420E-02
0.25	0.10	23.37741166	7.377873E-02
	0.20	24.37061285	7.532919E-02
	0.50	23.32079328	6.727035E-02
	0.80	26.02888669	5.521947E-02
	1.00	24.72410843	4.462950E-02
0.3	0.20	36.47451971	1.568466E-01
	0.50	36.48166279	1.433911E-01
	0.80	29.38410695	1.072913E-01
	1.00	35.96599918	8.500074E-02

One of the major objective of this study was to examine whether or not the dynamic properties of residual soil be influenced by the frequency or rate of loading. By comparing the shear modulus and damping ratio obtained from every test, it did not show significant trends to prove that the shear modulus and damping ratio are affected by the frequency. This can be shown from the graph of shear modulus vs frequency and damping ratio vs frequency below.

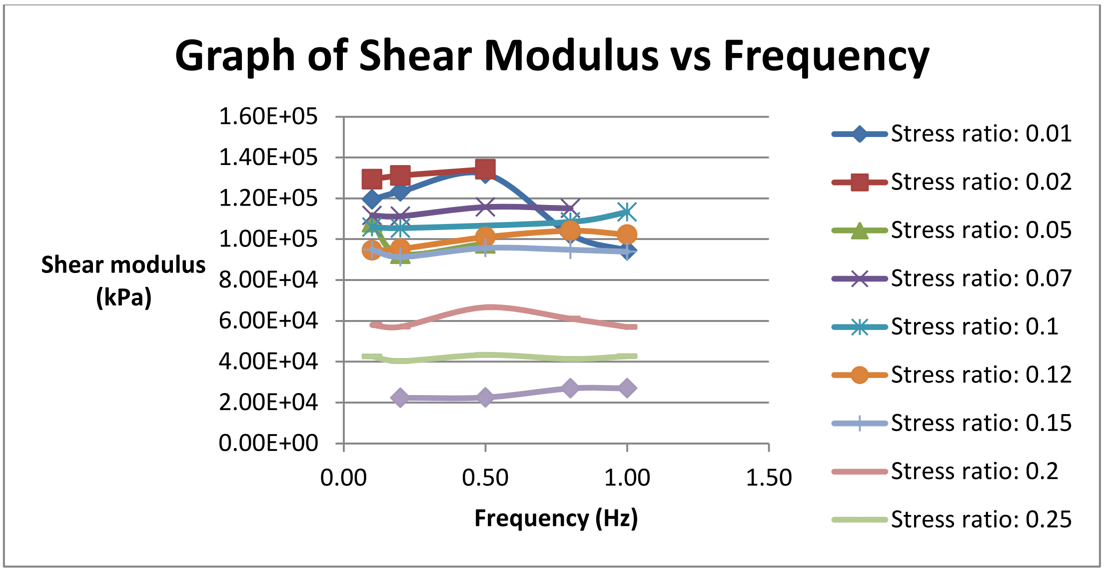

Figure 4.1: Graph of Shear Modulus vs Frequency

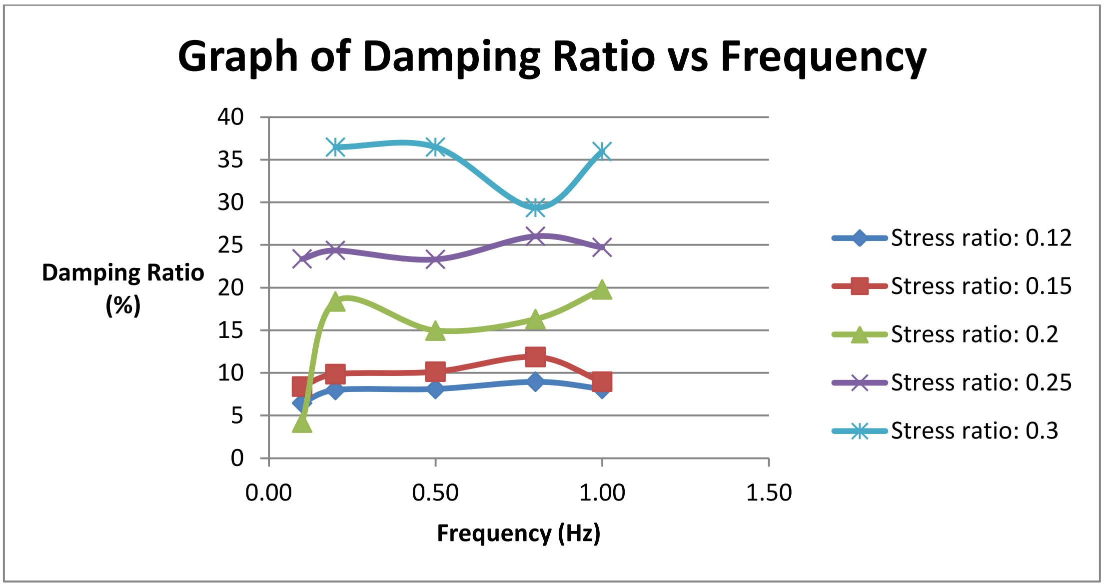

Figure 4.2: Graph of Damping Ratio vs Frequency

In addition, as the stress ratio increases, the shear modulus will reduce, whereas the damping ratio will increase with the increase of stress ratio. This behaviour is shown on the figures below.

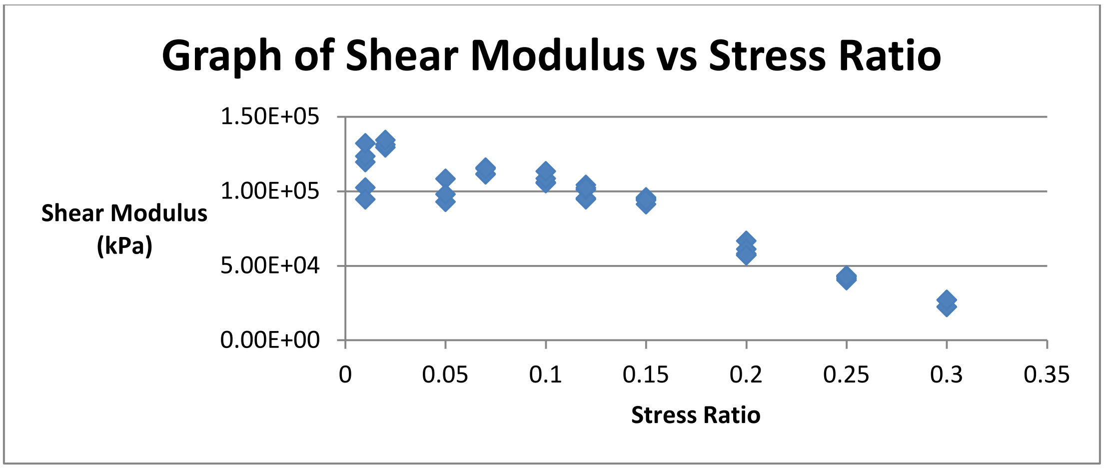

Figure 4.3: Graph of Shear Modulus vs Stress Ratio

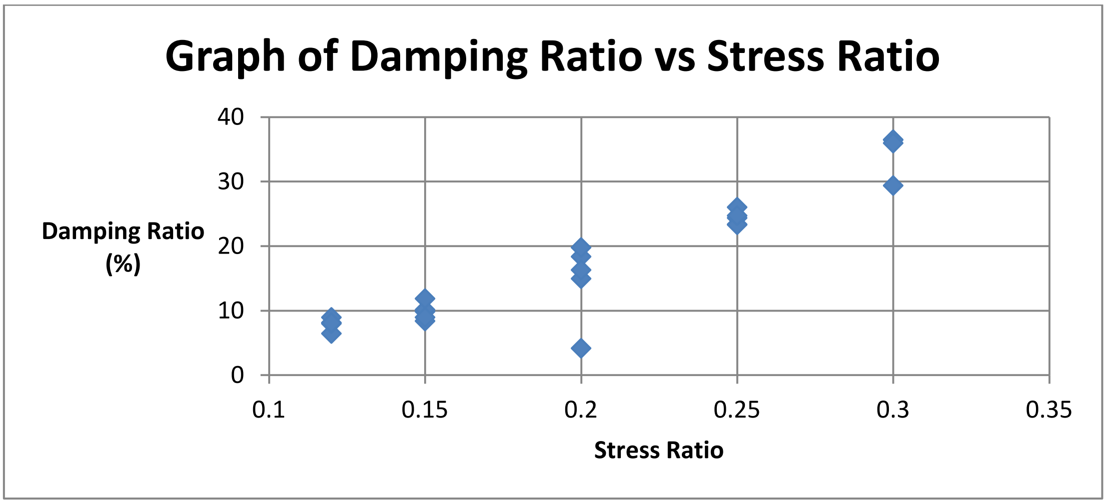

Figure 4.4: Graph of Damping Ratio vs Stress Ratio

The graph of shear modulus vs stress strain and the graph of damping ratio vs shear strain are plotted too. They are shown below.

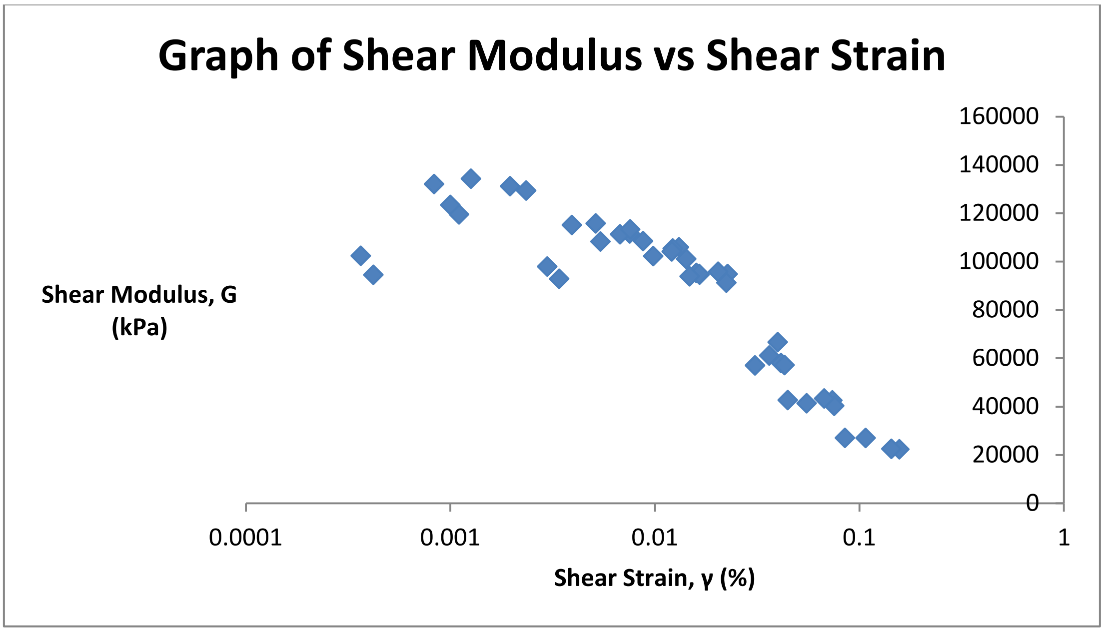

Figure 4.5: Graph of Shear Modulus vs Shear Strain

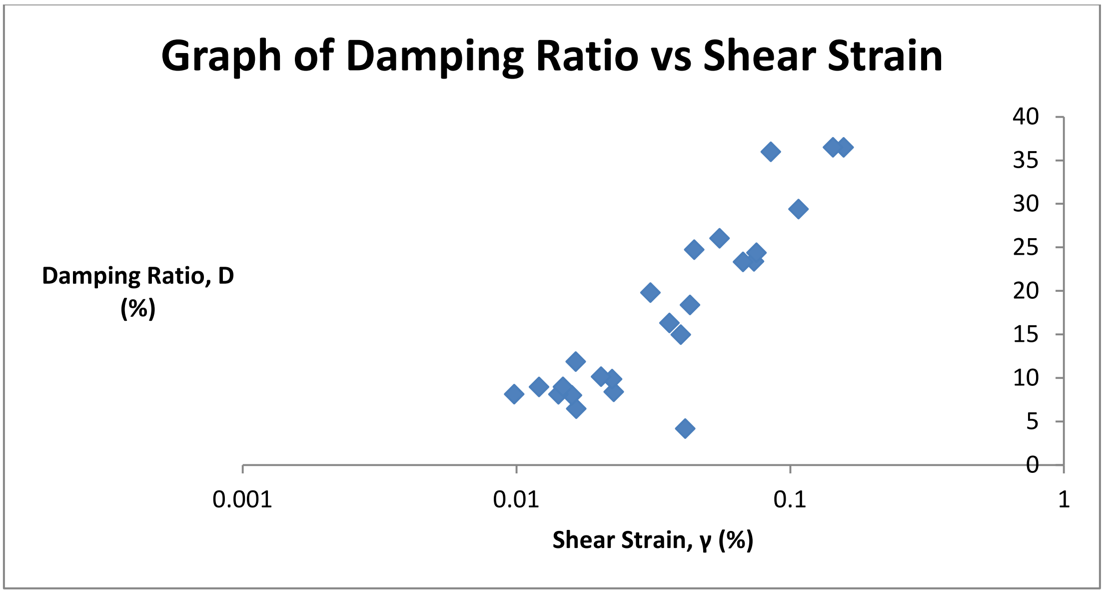

Figure 4.6: Graph of Damping Ratio vs Shear Strain

Besides that, the graph of shear strain vs frequency is also plotted and shown below. The y-axis is set to logarithmic scale. From this graph, it shows that the shear strain will reduce with the increase of frequency.

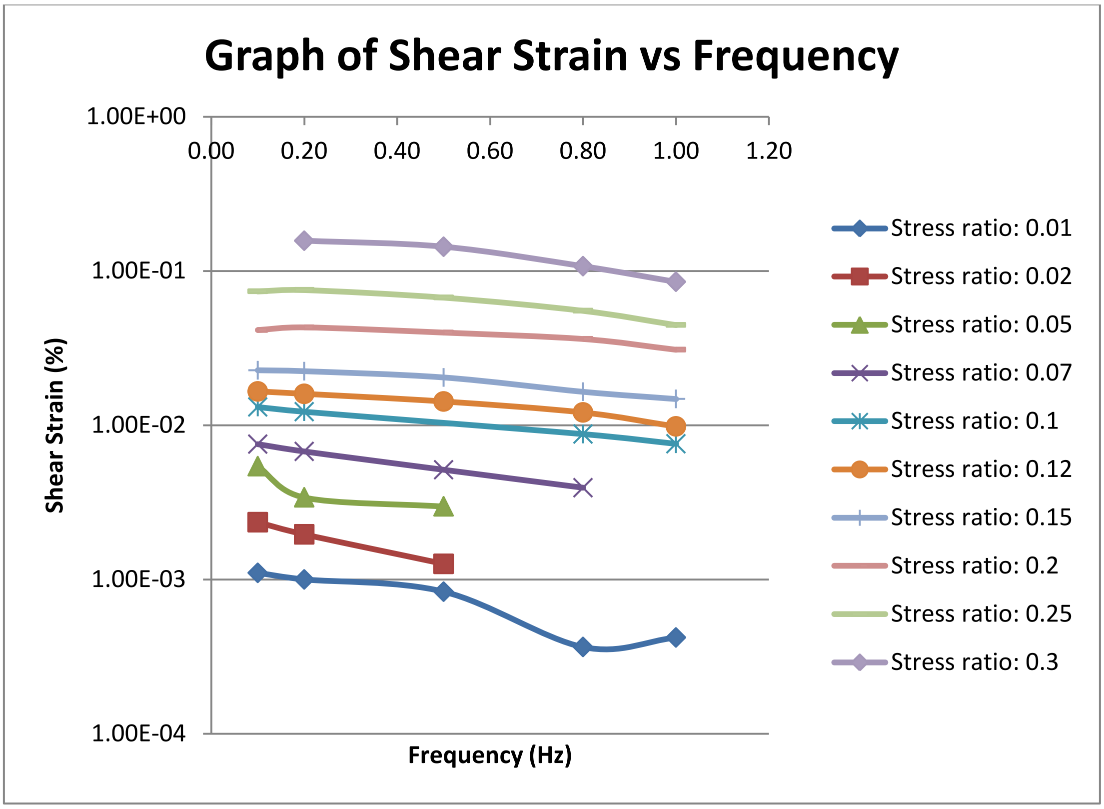

Figure 4.7: Graph of Shear Strain vs Frequency

4.3 Discussion

After all the data is obtained from the cyclic triaxial test, the author observed that some of the data are not suitable to be used. The summary is shown in the table below.

Table 4.3: Error with Data

		Frequency				
		0.1	0.2	0.5	0.8	1
Stress Ratio	0.01					
	0.02				No reading	No reading
	0.05				Only compression	Only compression
	0.07					Only compression
	0.10			Weird deformation		
	0.12					
	0.15					
	0.20					
	0.25					
	0.30	Weird deformation				
	0.35	LDT loosen	LDT loosen	LDT loosen	LDT loosen	LDT loosen

The error written "No reading" means there is response recorded from the sensors during testing. On the other hand, the error "Only compression" means that the cyclic loading is only acting on the compression side. Other than that, the error "Weird deformation" indicates that the deformation recorded is either extremely high or low, this might due to the problem with the sensors. In addition, the error "LDT loosen" means that the strain is too high for LDT to measure and the position of LDT is already affected.

By plotting the graph of stress ratio vs axial strain for both LDT and LVDT, it is very obvious that the difference between both sensors are too large. One of the graph is illustrated in the below. Since the difference is so large, the data from one of the sensor has to be chosen to represent the strain of the soil sample. The LDT is chosen because that the LDT is attached directly to the soil sample that measure the strain of the sample directly and the LVDT is measuring the strain from the piston.

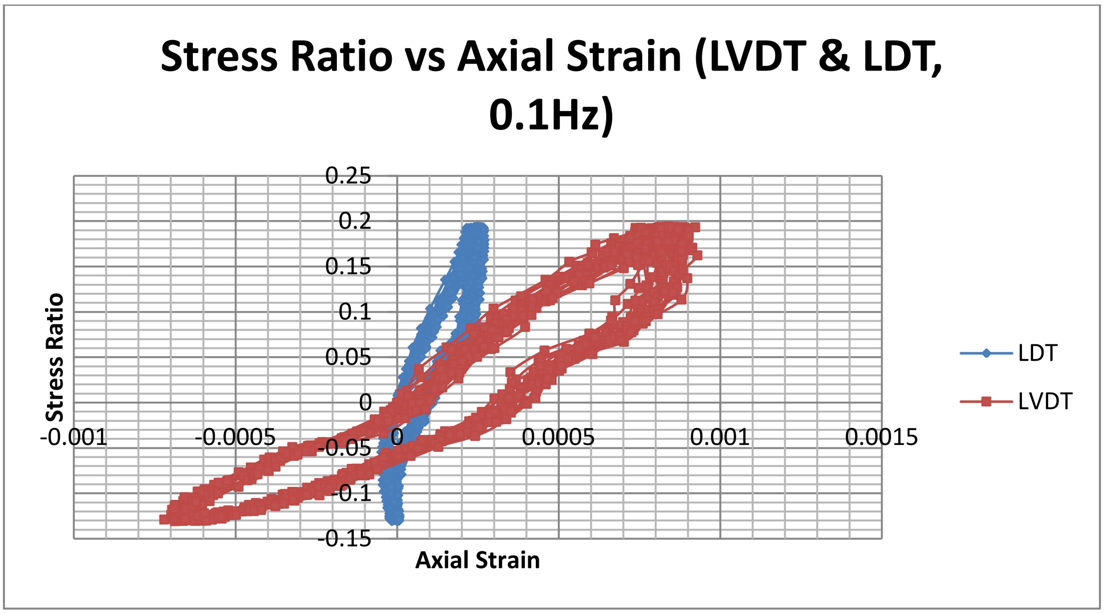

Figure 4.8: Graph of Stress Ratio vs Axial Strain

Other than that, by comparing the graph of stress ratio vs axial strain at low stress ratio, such as 0.01, it shows that the LDT is more sensitive compared to LVDT. From the graphs below, LVDT did not react to the load at all, whereas the LDT still show some reaction and shear modulus can still be obtained from LDT.

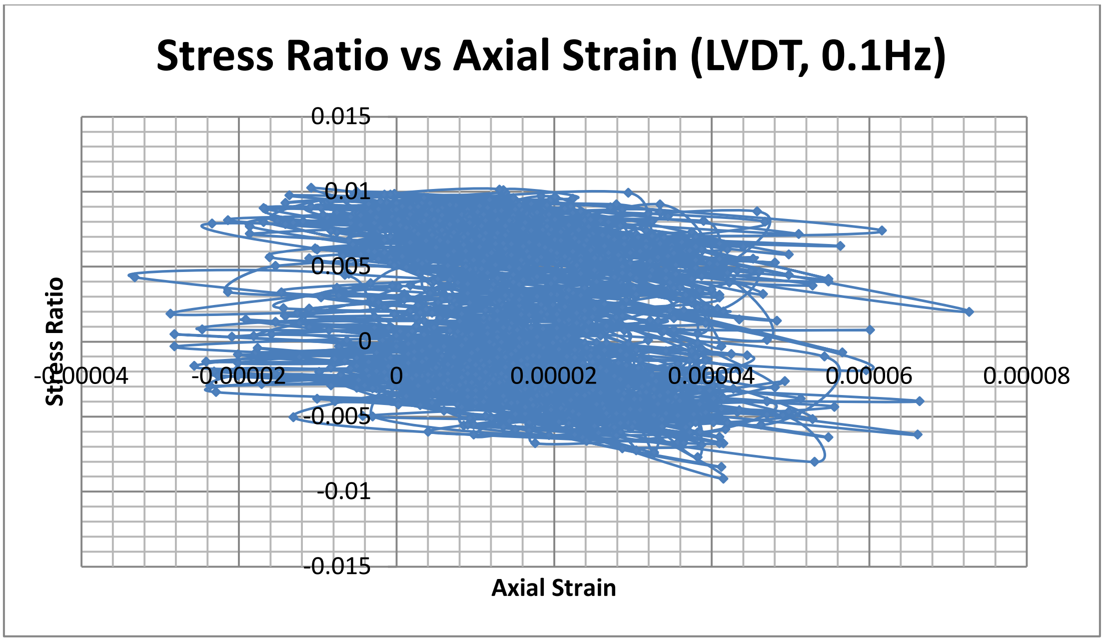

Figure 4.9: Sensitivity of LVDT

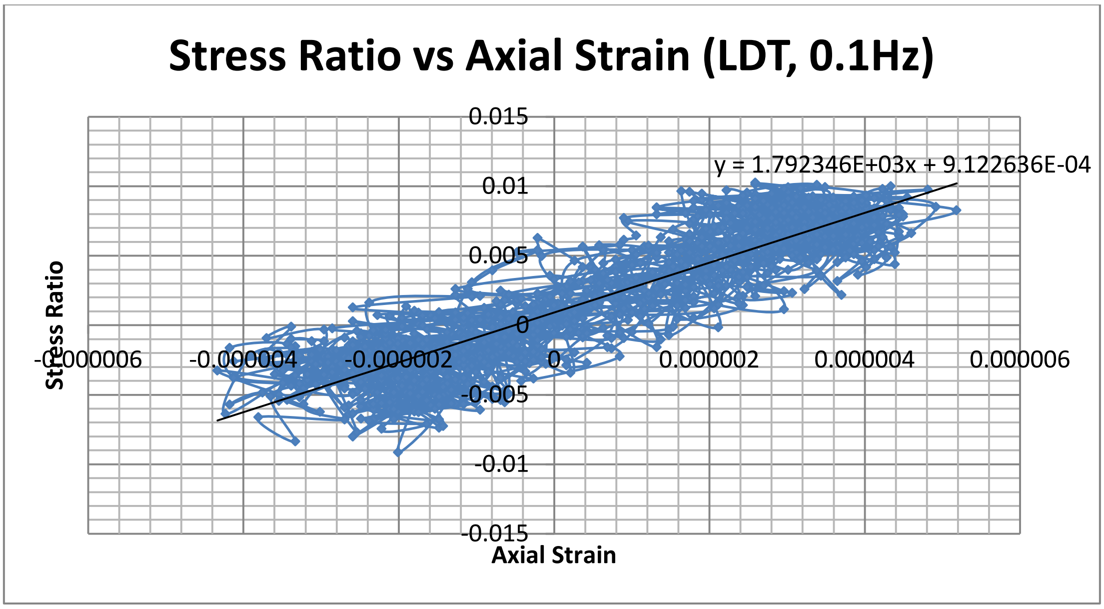

Figure 4.10: Sensitivity of LDT

From the graph above, it shows that LDT can measure up to the strain of 10^{-6}, whereas LVDT is not able to do it. Therefore, LDT is more reliable compared to LVDT.

By looking at the graph of stress ratio vs axial strain of LDT, for low stress ratio, such as 0.01 to 0.10, no loop can be seen. For stress ratio after 0.12, the loop is getting more and more obvious. Therefore, the soil can be said to be in the state of elastic from stress ratio 0.01 to 0.10. However, after 0.12, the soil started to become elasto-plastic.

Based on the study on Singapore residual soil by Tou (2003), the results are compared with the residual soil studied by the author. Two different soils are tested by Tou (2003). They are the Jurong Formation residual soils and Bukit Timah Granite residual soil. Two samples are obtained from Jurong Formation residual soils and labelled as JF1 and JF2, whereas the sample of Bukit Timah Granite residual soils is labelled as BT. The basic index properties of all three soils are listed in the table below.

Table 4.4: Basic Index Properties of JF and BT soils (Tou, 2003)

Parameters	Jurong Formation		Bukit Timah Granite
	JF1	JF2	BT
Gravel (%)	0		0
Sand (%)	32		63
Silt and clay (%)	68		37
Plastic limit, PL (%)	30		32
Liquid limit, LL (%)	55		55
Plasticity index, PI (%)	25		23
Specific gravity, ρ_s	2.71		2.62
USCS symbol	CH		SC
Bulk density, ρ_b (Mg/m^3)	1.926	1.917	2.434
Dry density, ρ_d (Mg/m^3)	1.547	1.543	1.928
Void ratio, e	0.752	0.756	0.357
Initial degree of saturation, S (%)	88	87	100
Initial water content, w (%)	24.5	24.2	26.3

The residual soil from sedimentary Jurong Formation (JF1 and JF2) is classified as CH in Unified Soil Classification System (USCS), whereas the residual soil of Bukit Timah Granite (BT) is classified as SC, with significant sand content.

Besides, the experimental parameters for soil specimens JF1, JF2 and BT are listed in the table below.

Table 4.5: Experimental Parameters for Soil Specimens JF1, JF2 and BT (Tou, 2003)

Sample Identification Number	Jurong Formation		Bukit Timah Granite
	JF1	JF2	BT
Cell pressure (kPa)	390	290	290
Back pressure (kPa)	368	243	261
Effective confining pressure (kPa)	32	47	28
Final B-value	0.82	0.84	0.92

Tou (2003) concluded that the shear modulus reduces with the increase of shear strain. This result shows the same trend found by the author on Shah Alam residual soil. The figures below show the graph of shear modulus vs shear strain for JF1, JF2 and BT from Tou (2003).

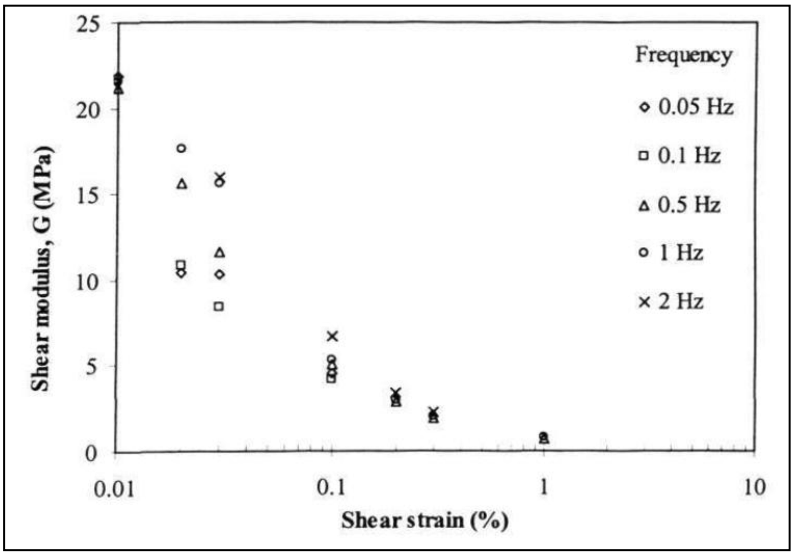

Figure 4.11: Graph of Shear Modulus vs Shear Strain for JF1 at 390 kPa Consolidation Pressure (Tou, 2003)

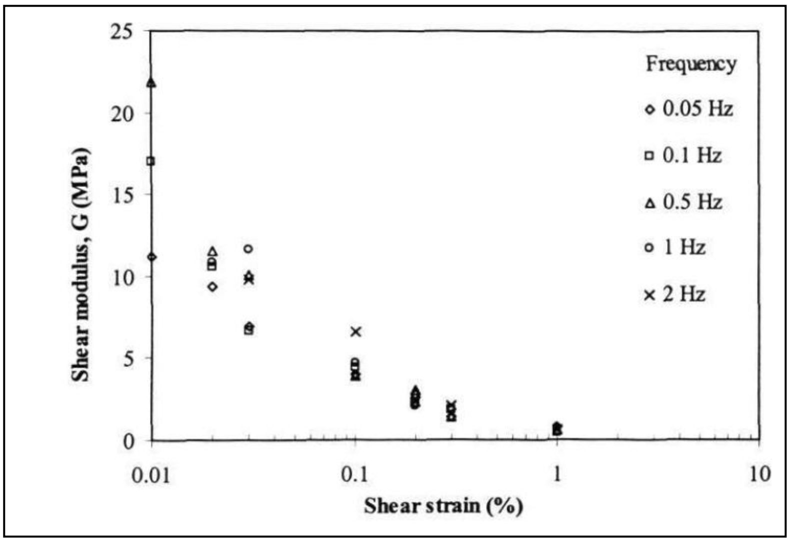

Figure 4.12: Graph of Shear Modulus vs Shear Strain for JF2 at 290 kPa Consolidation Pressure (Tou, 2003)

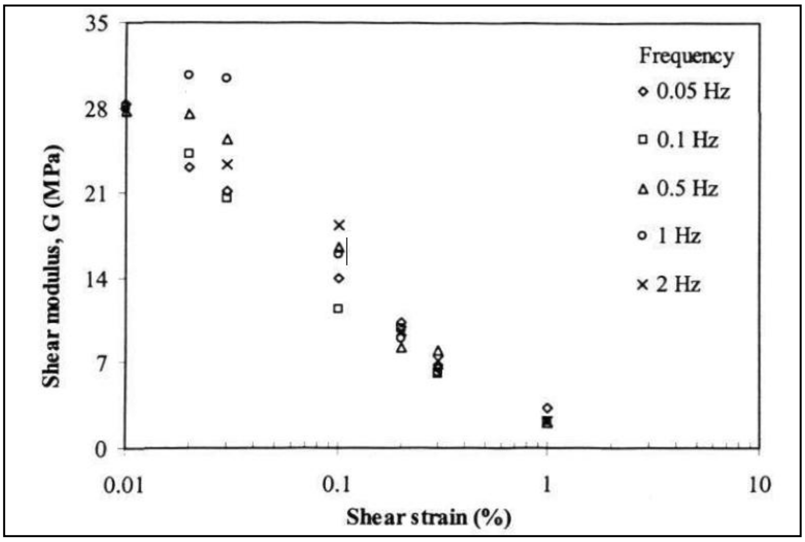

Figure 4.13: Graph of Shear Modulus vs Shear Strain for BT at 290 kPa Consolidation Pressure (Tou, 2003)

On the other hand, Tou (2003) also presents that the damping ratio increases as shear strain decreases for Singapore residual soil. This shows the same relationship as the result from the author on Shah Alam residual soil. Figures below show the graph of damping ratio vs shear strain of JF1, JF2 and BT.

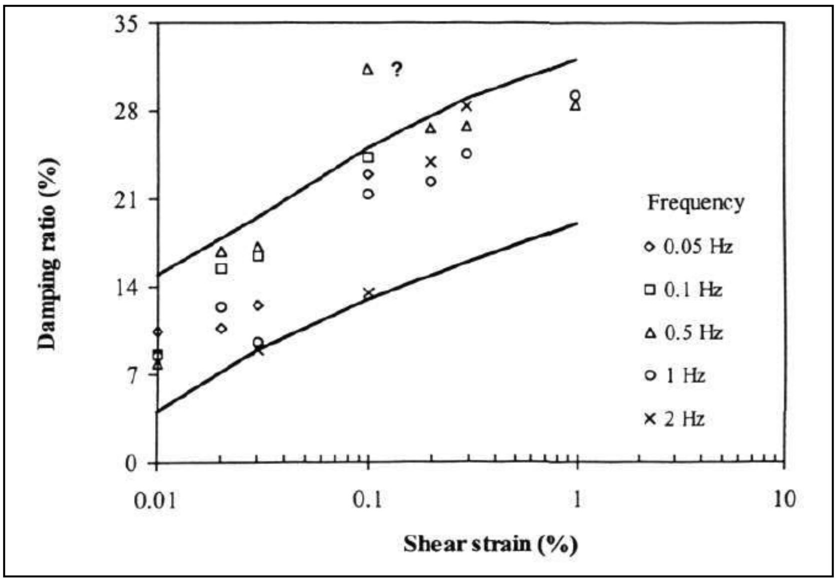

Figure 4.14: Graph of Damping Ratio vs Shear Strain for JF1 at 390 kPa Consolidation Pressure (Tou, 2003)

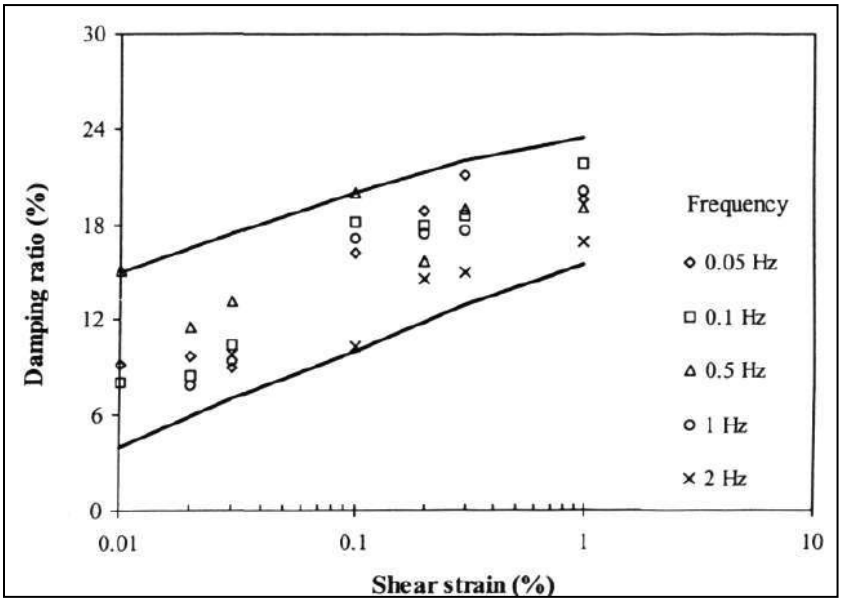

Figure 4.15: Graph of Damping Ratio vs Shear Strain for JF2 at 290 kPa Consolidation Pressure (Tou, 2003)

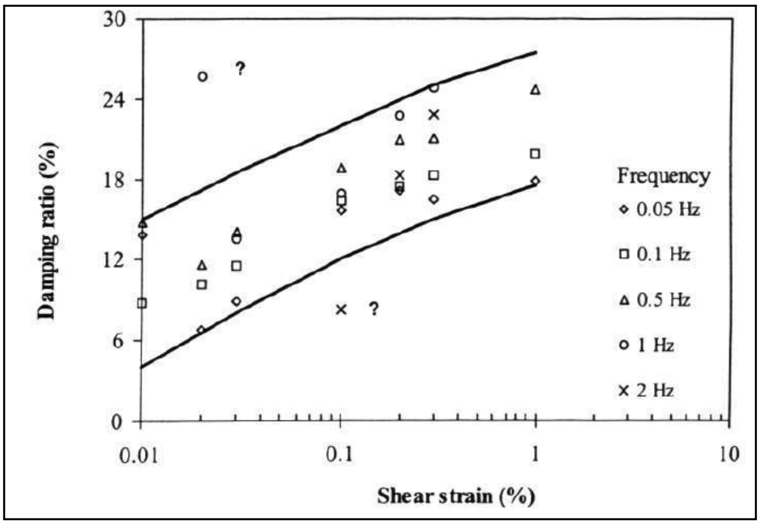

Figure 4.16: Graph of Damping Ratio vs Shear Strain for BT at 290 kPa Consolidation Pressure (Tou, 2003)

Other than that, the Tou (2003) also commented that the shear modulus and damping ratio at certain shear strain level increase as the frequency increases. This is more obvious at small shear strain levels like 0.01 %, 0.02 % and 0.03 %. However, the author observed no significant trend from Shah Alam residual soil to prove that the frequency is affecting the shear modulus and damping ratio. From Tou's graph, not all the data shows the increase of shear modulus and damping ratio with the increase of frequency including some of the low shear strain level that is mentioned by Tou (2003). There are still some fluctuations and the amount of fluctuation is almost the same as the result obtained by the author for Shah Alam residual soil. The figures below show the graph of shear modulus and damping ratio vs frequency by Tou (2003).

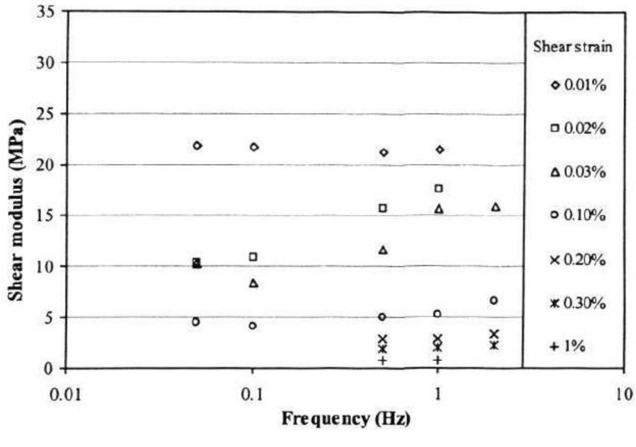

(a) Shear Modulus

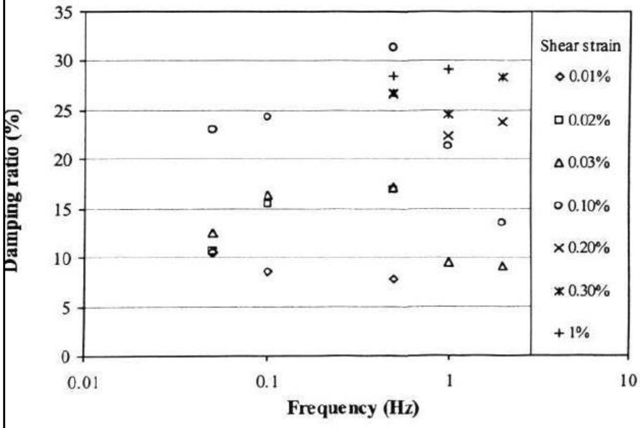

(b) Damping ratio

Figure 4.17: Graph of Shear Modulus and Damping Ratio vs Frequency for JF1

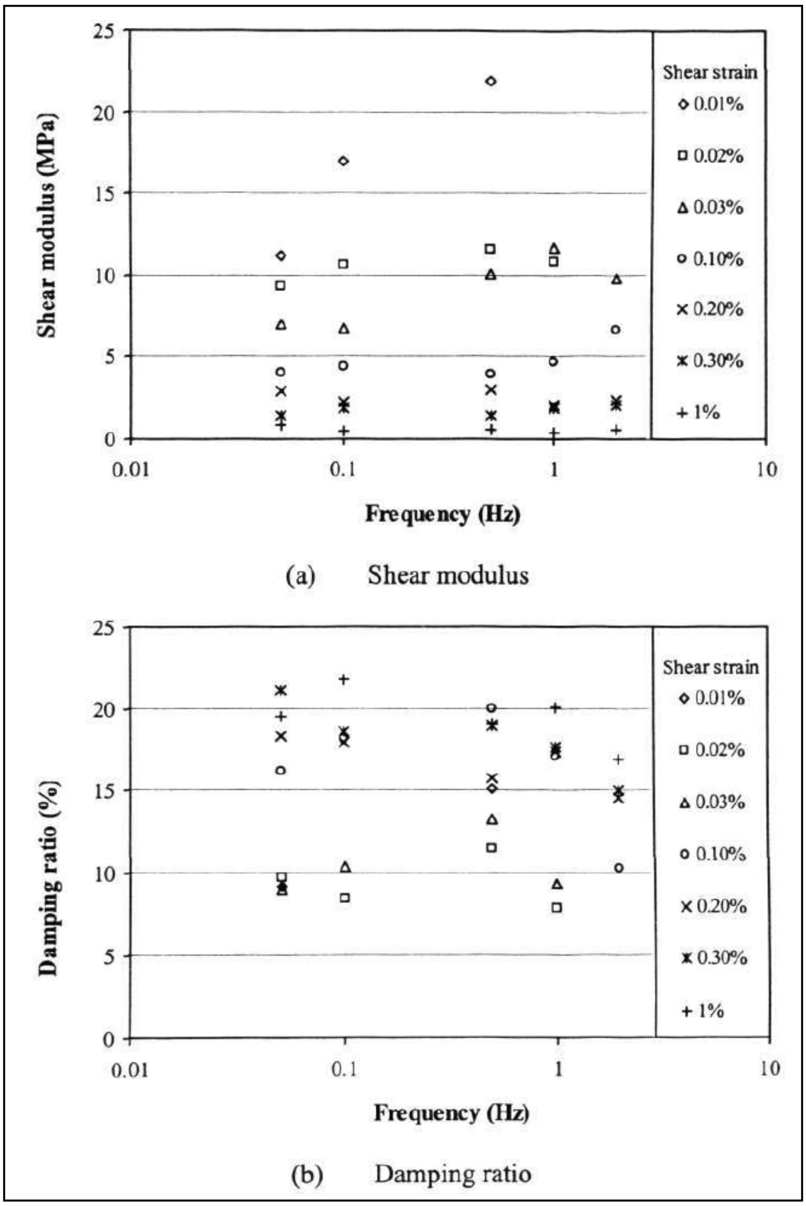

Figure 4.18: Graph of Shear Modulus and Damping Ratio vs Frequency for JF2

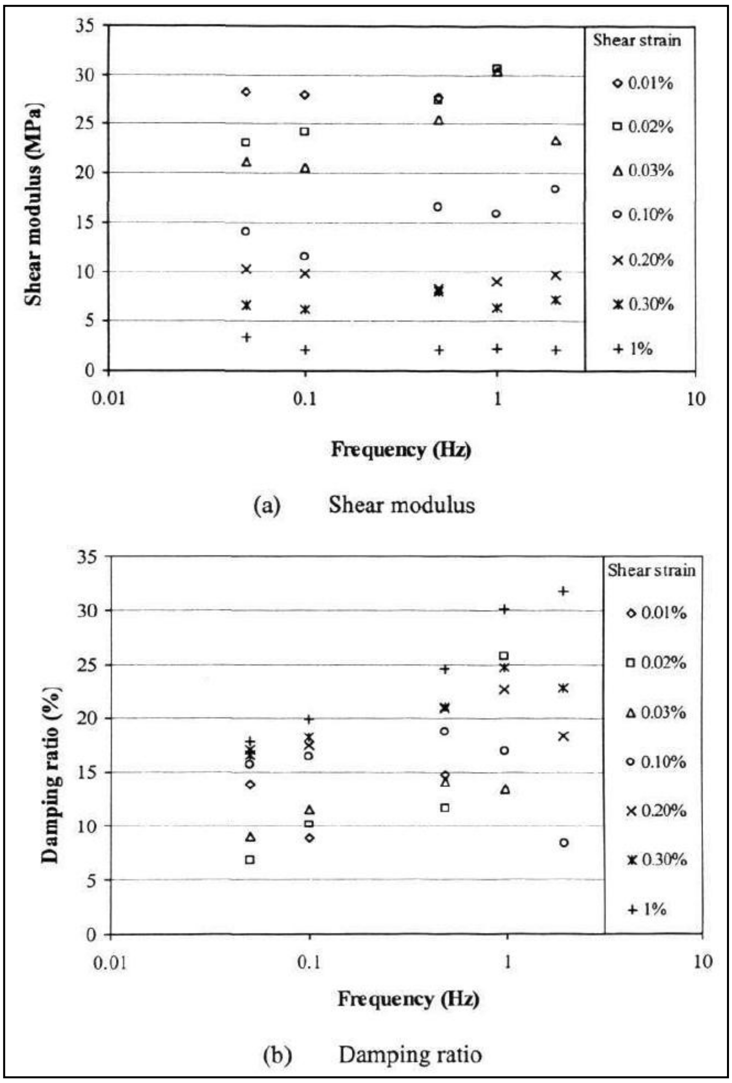

Figure 4.19: Graph of Shear Modulus and Damping Ratio vs Frequency for BT

In addition, the author also plotted a graph of shear modulus vs shear strain together with the result obtained from Tou (2003). The result of JF2 is chosen to be compared with the result of the residual soil in Shah Alam because JF2 has lesser technical problems occurred when the test is conducted (Tou, 2003). However, the effective confining pressure of JF2 is only 47 kPa, whereas the confining pressure of this research is 100 kPa. The relationship between the shear modulus and the confining pressure can be expressed in the formula below (Ishihara, 1996).

$$G = AF(e)\sigma_c^{\ n} \tag{4.1}$$

where

G = shear modulus, MPa

A = constant

$F(e)$ = function of e

σ_c = confining pressure, MPa

n = constant

By assuming the constant A and the function $F(e)$ are the same for both JF2 and Shah Alam residual soil, whereas the constant n is 0.5, the shear modulus of JF2 can be converted to 100 kPa confining pressure with the modified equation below.

$$G_1 = G_0 \frac{{\sigma_{c1}}^{0.5}}{{\sigma_{c0}}^{0.5}} \tag{4.2}$$

where

G_1 = new shear modulus, MPa

G_0 = initial shear modulus, MPa

σ_{c1} = new confining pressure, MPa

σ_{c0} = initial confining pressure, MPa

The converted data for JF2 is shown in the table below.

Table 4.6: JF2 Converted Result

	Confining Pressure		
	47	100	
Frequency (Hz)	Shear Modulus, G (MPa)	Shear Modulus, G (MPa)	Shear Strain (%)
0.05	11.20	16.34	0.01
0.10	17.02	24.83	0.01
0.50	21.90	31.94	0.01
0.05	9.36	13.65	0.02
0.10	10.62	15.49	0.02
0.50	11.54	16.83	0.02
1.00	10.81	15.77	0.02
0.05	6.97	10.17	0.03
0.10	6.70	9.77	0.03
0.50	10.09	14.72	0.03

1.00	11.62	16.95	0.03
2.00	9.83	14.34	0.03
0.05	4.00	5.83	0.10
0.10	4.42	6.45	0.10
0.50	3.91	5.70	0.10
1.00	4.70	6.86	0.10
2.00	6.60	9.63	0.10
0.05	2.77	4.04	0.20
0.10	2.27	3.31	0.20
0.50	3.00	4.38	0.20
1.00	2.09	3.05	0.20
2.00	2.38	3.47	0.20
0.05	1.42	2.07	0.30
0.10	1.85	2.70	0.30
0.50	1.36	1.98	0.30
1.00	1.89	2.76	0.30
2.00	2.05	2.99	0.30
0.05	0.80	1.17	1.00
0.10	0.43	0.63	1.00
0.50	0.60	0.88	1.00
1.00	0.41	0.60	1.00
2.00	0.60	0.88	1.00

Figure 4.20 and 4.21 are produced to compare the shear modulus from Tou (2003) and this research by author. Figure 4.20 shows a direct comparison of the shear modulus of JF2 with confining pressure of 47 kPa while the confining pressure of 100 kPa is used in this research. In order to compare the shear modulus with the same confining pressure, the shear modulus of JF2 was adjusted to 100 kPa as shown above. Figure 4.21 below shows the comparison of shear modulus at the same confining pressure of 100 kPa.

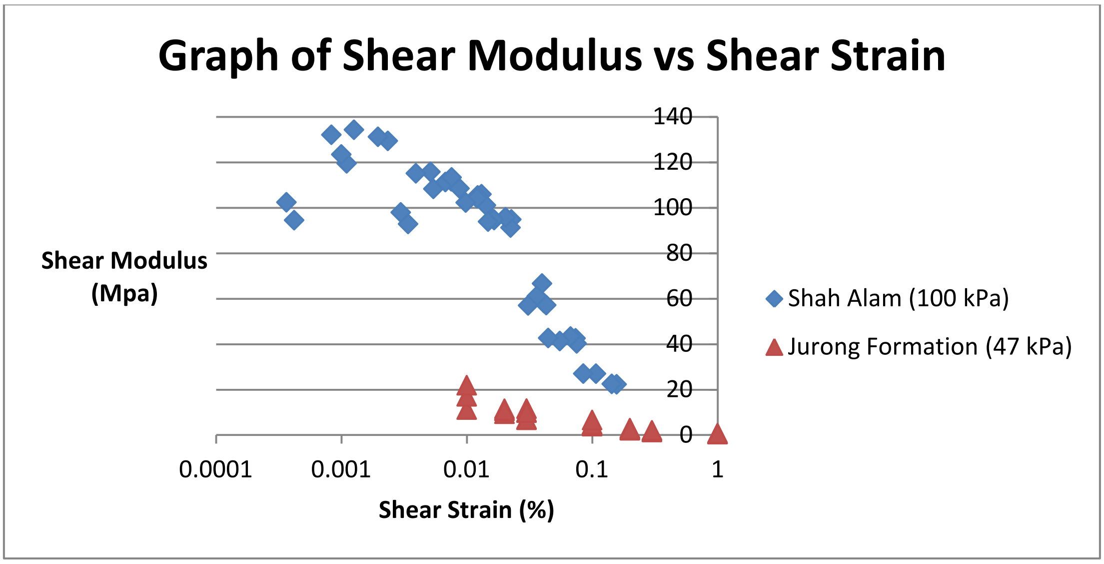

Figure 4.20: Comparing with JF2 (47 kPa)

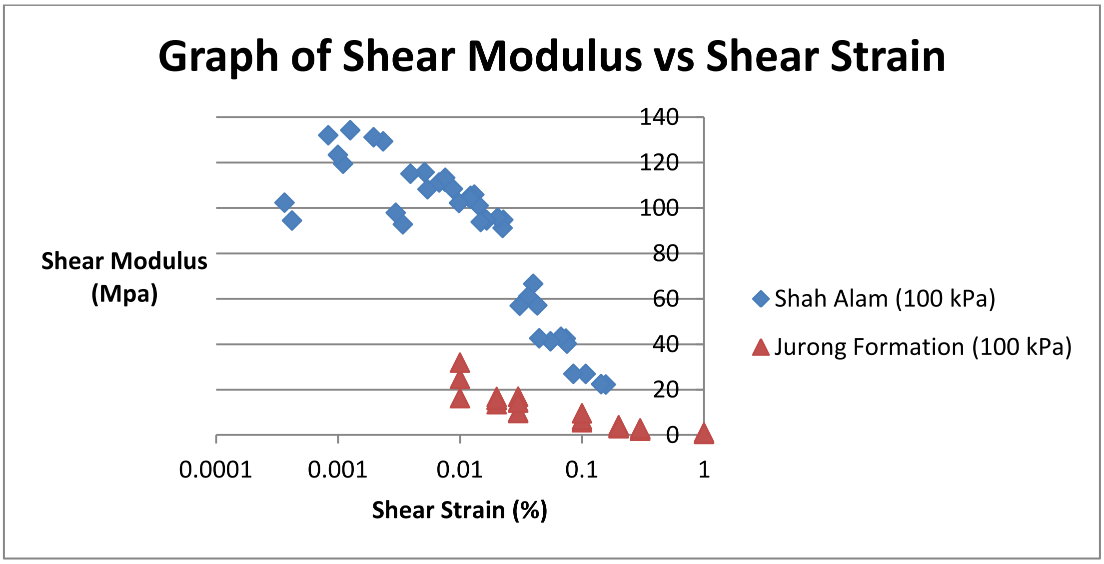

Figure 4.21: Comparing with JF2 (100 kPa)

From these two figures, it is clearly shown that the shear modulus of the residual soil from Shah Alam has much higher shear modulus compare to the JF2 soil in Singpoare.

4.4 Problems Encountered

In this section, all problems encountered by the author during this research will be explained with the solutions. The major problem is the noise received by the USB-6210 device from the sensors. This can really affect the result as the value is very unstable. The noise can be generated from all kinds of electronic devices such as laptop, power source, transformer, and amplifier.

This problem can be solved by grounding all the electronic devices. The laptop can be grounded by using a USB cable and modified it with the other end replaced by a crocodile clip. This cable can be plugged into the laptop easily and the other end can be clipped to the transformer chassis. The transformer is also grounded by connecting a wire to the chassis and the ground wire that is plugged into the power supply. This creates a continuous flow and every electronic devices can be grounded by simply connected to the chassis of the transformer.

To obsolete the noise from the laptop power supply, the power supply can be turned off when the test carrying out. However, a constant check should be taken on the laptop battery level to prevent the laptop from turning off in the process of testing.

In addition, there is also another problem with the LDT waterproofing. The author tested the LDT in the water but the reading shows a very unstable value. Therefore, the LDT is recoated with another layer of glue and a layer of paint is sprayed on the wire connections. However, the LDT still failed to response normally when submerged into the water. This problem is solved by consolidating the sample with just the air pressure supplying to the triaxial cell without introducing water to the cell.

Figure 4.22: LDT is Wrapped Up for Painting

Besides, some wire connections are easily be broken off. To solve this problem, epoxy is used to cover the fragile part of the connection. Other than that, epoxy is also used to seal the cable inside the water tank to prevent any leakage.

Plus, sometimes the LDT cannot be adjusted to the initial position, which is 1 mm deformation. To solve this problem, if the LDT is deformed less than 1 mm, a hard plastic material can be placed in the clip to increase the deformation of LDT. Therefore, it is always better to attach the LDT with the deformation lesser than 1 mm than more than 1 mm.

Other than that, if the specimen mould is not applied with oil, the soil sample can be broken into half when removing the mould. Therefore, it is always advisable to apply a layer of oil on the mould before compacting the soil.

Figure 4.23: Soil Sample Broken into Half

CHAPTER 5

CONCLUSIONS AND RECOMMENDATIONS

5.1 Conclusions

In conclusion, the frequency did not affect the shear modulus and damping ratio of the residual soil tested herein. It was clearly shown that the shear modulus decreases with the increase of stress ratio, whereas the damping ratio increases with the increase of stress ratio. The relationship between shear modulus vs shear strain and damping ratio vs shear strain of the tested residual soil is obtained.

5.2 Recommendations

To improve the quality of this research in the future, there are several things that need to be improved. First of all, the Data Acquisition program and Air Pressure Controller program need to be improved. This two programs are included in the CD attached to this report. The data acquisition speed should be increased to obtain more data, which will eventually provide a better result for high frequency test.

For the Air Pressure Controller program, the maximum frequency it can go is 1 Hz. If a higher frequency is used, the number of cycle performed will be lesser than the cycle intended to perform due to some delay. This problem should be solved in order to run the cyclic test with frequency higher than 1 Hz.

Plus, the LDT waterproofing should be improved as well. This might be done by using epoxy to replace all the existing glue since epoxy is much stronger than the glue. However, other better alternative can be used as well, because once the epoxy is used, it will be permanent. Therefore, it is difficult to do some modification on the connection in the future if needed.

Last but not least, a bigger space is needed for this research. The current space is too small and everything has to be crammed together in a small space, which is quite untidy.

REFERENCES

Boon, T. Y. (2013). *Disaster risk reduction in malaysia and earthquake study based on cyclic triaxial test.* BSc thesis, Universiti Tunku Abdul Rahman.

British Standards Institution (1990). BS 1377-2:1990. *Soils for civil engineering purposes. Classification tests.* London: BSI.

Doris, A. M. Y. and Hafez, M. A. (2011). 'Static laboratory compaction method', *Electronic Journal of Geotechnical Engineering*, vol. 16, pp. 1589-1593.

Geotechnical Laboratory of DGM, (2004). *Soil mechanics laboratory manual.*

Jennifer, L. D., Jonathan, D. B., and Michael F. R. (2007). *The liquefaction susceptibility, resistance, and response of silty and clayey soils.*

Ishihara, K., (1996). *Soil behaviour in earthquake geotechnics,* Oxford University Press, New York, pp. 87.

Martin, D. L. (1990). *A laboratory study of the effect of stress state on the elastic moduli of sand.* PhD thesis, The University of Texas at Austin.

Pieter, K. S. (1992). *Implementation of a resonant column/torsional shear testing apparatus.* MSc thesis, North Carolina State University.

Rosaidi, C. A. (2001). 'Earthquake monitoring in malaysia'. Paper presented at the Seismic Risk Seminar, Malaysia.

Sitharam, T. G. (2004). 'Dynamic properties and liquefaction potential of soils', *Current Science*, vol. 87, no. 10, pp. 1370.

Sherliza, Z. S., Sumio, S., and Hiroyuki, G. (2012). 'Proposal for seismic resistant design in malaysia: assessment of possible ground motions in peninsular malaysia', *Annual Report of Disaster Prevention Research Institute Kyoto University*, no. 55b.

Tou, J. H. (2003). *Cyclic triaxial test apparatus for evaluating dynamic properties of residual soils.* MSc thesis, Nanyang Technological University.

Transducer Techniques, (n.d.). *Quater bridge, half bridge and full wheatstone bridge strain gauge load cell configurations.* Available from: <http://www.transducertechniques.com/wheatstone-bridge.aspx>. [19 April 2013].

APPENDICES

APPENDIX A: Calibration of Air Pressure Transducer

Air pressure (bar)	Voltage supply (v)	Voltage difference (v)
1	2.9	1.25879
1.5	3.5	1.85879
2	4.1	2.45879
2.5	4.7	3.05879
3	5.3	3.65879
3.5	5.95	4.30879
4	6.55	4.90879
4.5	7.2	5.55879
5	7.85	6.20879
4.5	7.2	5.55879
4	6.55	4.90879
3.5	5.95	4.30879
3	5.3	3.65879
2.5	4.7	3.05879
2	4.1	2.45879
1.5	3.5	1.85879
1	2.9	1.25879

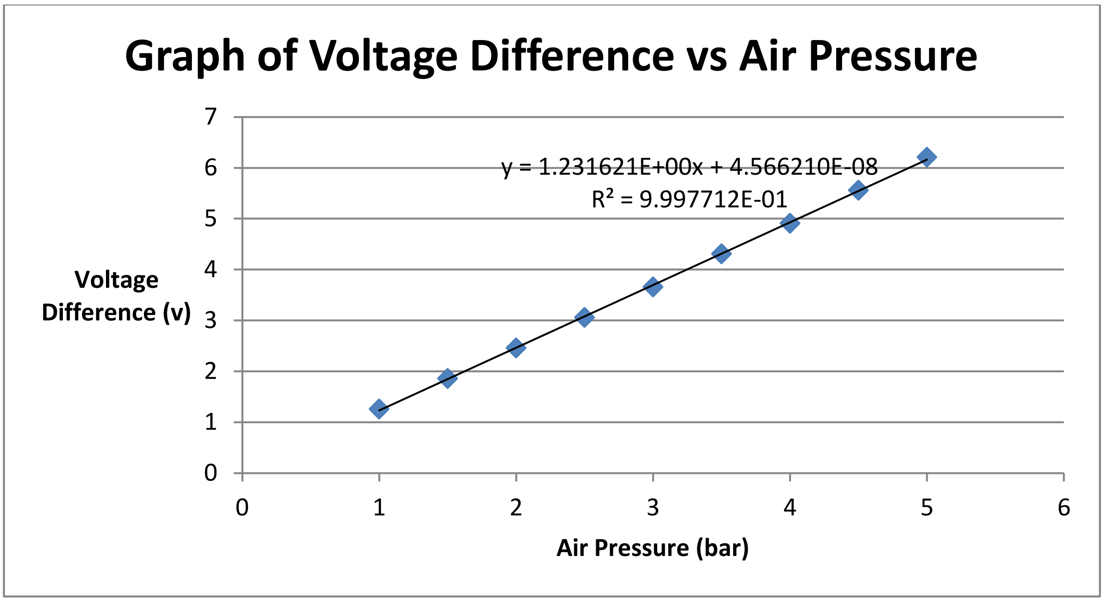

Graph of Voltage Difference vs Air Pressure
y = 1.231621E+00x + 4.566210E-08
R² = 9.997712E-01
Voltage Difference (v)
Air Pressure (bar)
0
1
2
3
4
5
6
7
0
1
2
3
4
5
6

APPENDIX B: Calibration of Load Cell Limit

Mass (kg)	Strain (με)	Strain (με)
0	39	0
4.988	10	-29
9.9825	-20	-59
14.9465	-53	-92
9.9825	-22	-61
4.988	9	-30
0	36	-3

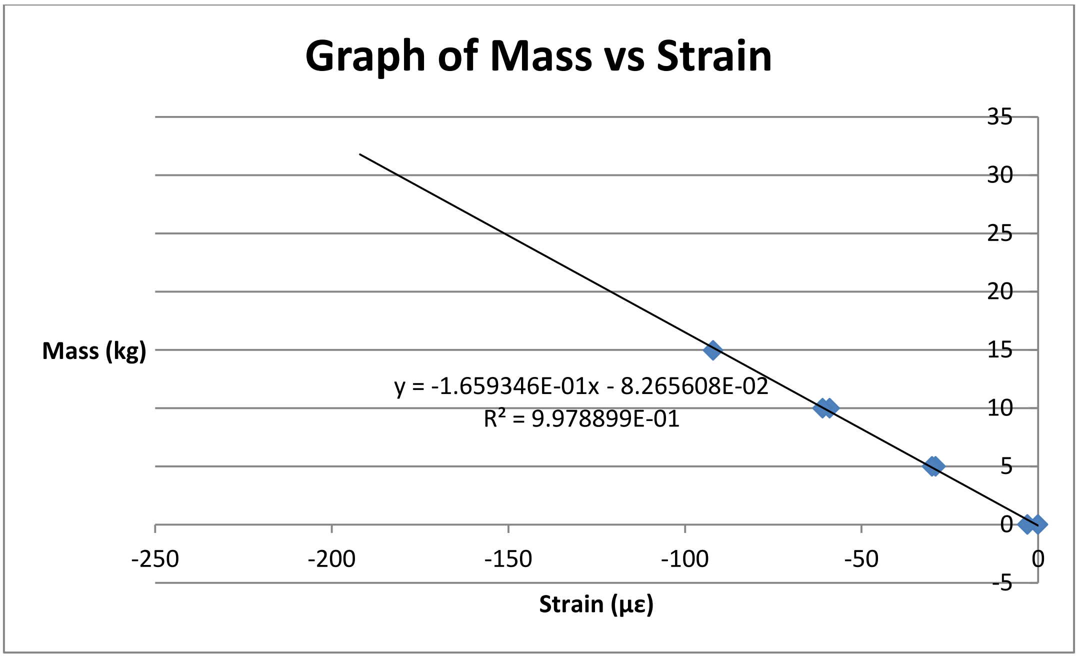

By using the equation from the graph, if maximum strain is 3000 με, then the load will be 497.72 kg.

APPENDIX C: Calibration of Load Cell

Mass (g)	Cumulative Mass (g)	Voltage (v)	Voltage Different (v)
0	0	4.58	-0.00194
10136.5	10136.5	4.22	-0.36194
9939	20075.5	3.87	-0.71194
10065	30140.5	3.5	-1.08194
9935	40075.5	3.14	-1.44194
9895	49970.5	2.78	-1.80194
9998	59968.5	2.42	-2.16194
4994.5	64963	2.25	-2.33194
4987.5	69950.5	2.14	-2.44194
4963	74913.5	1.96	-2.62194
4960	79873.5	1.79	-2.79194
4960	79873.5	1.79	-2.79194
4963	74913.5	1.95	-2.63194
4987.5	69950.5	2.12	-2.46194
4994.5	64963	2.29	-2.29194
9998	59968.5	2.47	-2.11194
9895	49970.5	2.82	-1.76194
9935	40075.5	3.18	-1.40194
10065	30140.5	3.53	-1.05194
9939	20075.5	3.89	-0.69194
10136.5	10136.5	4.25	-0.33194
0	0	4.6	0.01806

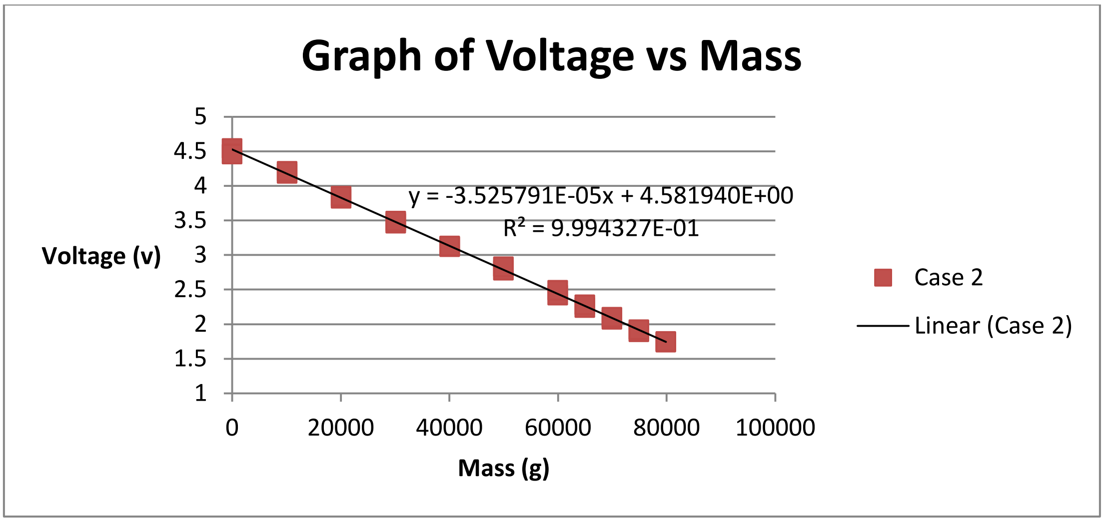
Graph of Voltage vs Mass
5
4.5
4
3.5
3
2.5
2
1.5
1
Voltage (v)
y = -3.525791E-05x + 4.581940E+00
R² = 9.994327E-01
0
20000
40000
60000
80000
100000
Mass (g)
Case 2
Linear (Case 2)

APPENDIX D: Calibration of Air Pressure Transducer with Load Cell

Air pressure (bar)	Voltage (v)	Mass of Load (g)	Mass of Load (kg)
0	4.54	0	0
0.5	3.66	24958.93829	24.95893829
1	2.83	48499.75509	48.49975509
1.5	2.03	71189.69899	71.18969899
2	1.25	93312.3943	93.3123943
2.5	0.37	118271.3326	118.2713326
2.5	0.27	121107.5756	121.1075756
2	0.98	100970.2504	100.9702504
1.5	1.9	74876.81488	74.87681488
1	2.68	52754.11957	52.75411957
0.5	3.58	27227.93268	27.22793268
0	4.46	2268.99439	2.26899439
0.5	3.64	25526.18689	25.52618689
1	2.81	49067.00369	49.06700369
1.5	1.95	73458.69338	73.45869338
2	1.12	96999.51018	96.99951018
2.5	0.27	121107.5756	121.1075756
2	1.14	96432.26158	96.43226158
1.5	1.88	75444.06347	75.44406347
1	2.73	51335.99808	51.33599808
0.5	3.36	33467.66726	33.46766726
0	4.28	7374.231768	7.374231768
0	4.36	5105.237378	5.105237378
0.5	3.59	26944.30838	26.94430838
1	2.71	51903.24668	51.90324668
1.5	1.91	74593.19058	74.59319058
2	1.07	98417.63167	98.41763167
2.5	0.27	121107.5756	121.1075756
2	0.98	100970.2504	100.9702504
1.5	1.81	77429.43357	77.42943357
1	2.65	53604.99247	53.60499247
0.5	3.56	27795.18128	27.79518128
0	4.43	3119.867287	3.119867287

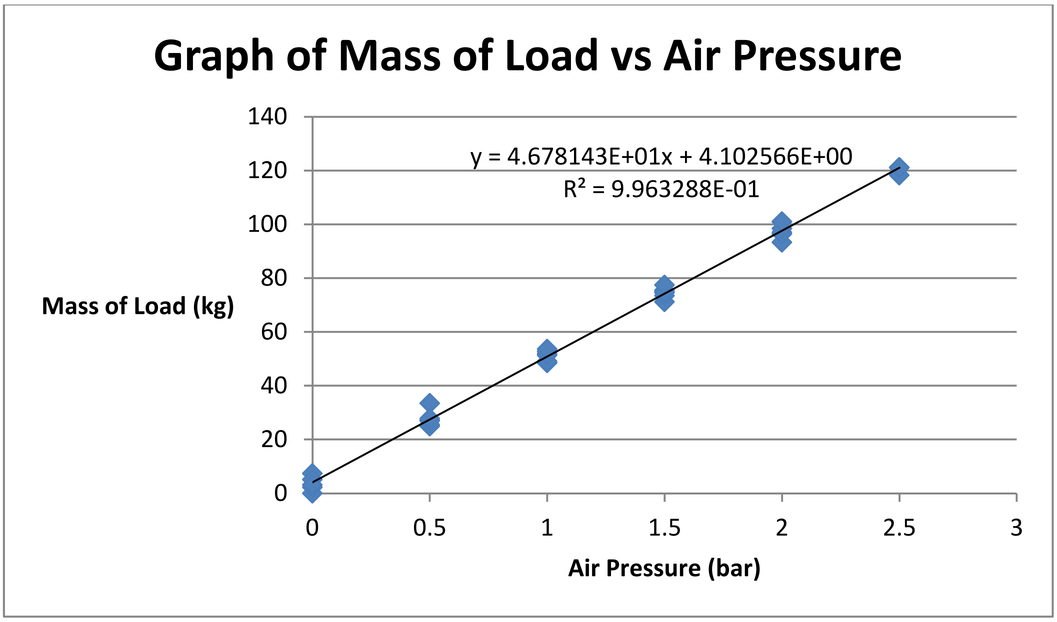
Graph of Mass of Load vs Air Pressure
y = 4.678143E+01x + 4.102566E+00
R² = 9.963288E-01
Mass of Load (kg)
Air Pressure (bar)
0
20
40
60
80
100
120
140
0
0.5
1
1.5
2
2.5
3

APPENDIX E: Calibration of LVDT

Dail gauge reading (0.01mm)	Voltage (v)
0	0.59
25	0.75
50	0.92
75	1.08
100	1.24
125	1.4
150	1.57
175	1.73
200	1.89
225	2.06
250	2.22
275	2.39
300	2.55
325	2.71
350	2.88
375	3.04
400	3.2
425	3.36
450	3.53
475	3.69
500	3.85
525	4.01
550	4.18
575	4.34
600	4.5
600	4.5
575	4.34
550	4.17
525	4.01
500	3.85
475	3.69
450	3.52

425	3.36
400	3.2
375	3.03
350	2.87
325	2.7
300	2.54
275	2.38
250	2.21
225	2.05
200	1.89
175	1.72
150	1.56
125	1.39
100	1.23
75	1.07
50	0.91
25	0.75
0	0.58
0	0.58
25	0.74
50	0.91
75	1.07
100	1.23
125	1.39
150	1.56
175	1.72
200	1.88
225	2.05
250	2.21
275	2.38
300	2.54
325	2.7
350	2.87
375	3.03
400	3.2
425	3.36
450	3.52
475	3.69
500	3.84
525	4.01
550	4.17

575	4.33
600	4.5

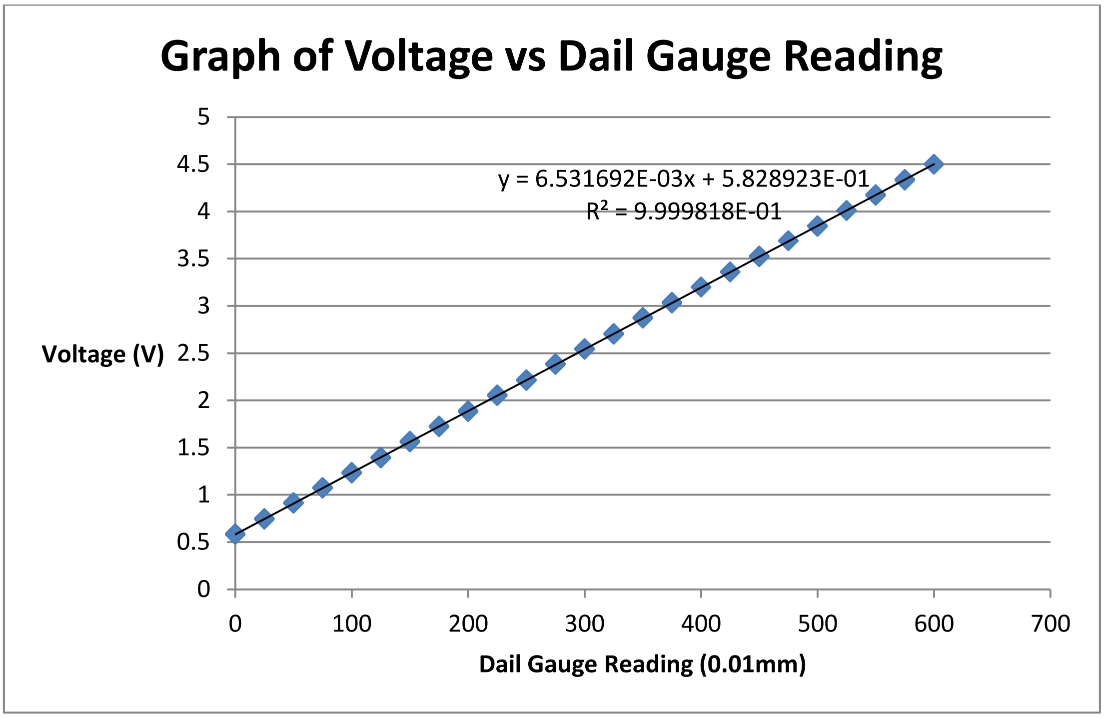

APPENDIX F: Calibration of LDT Initial Position

Dail gauge reading (0.01mm)	Strain (με)
0	-585
15	-122
30	430
45	931
60	1364
75	1715
90	2014
105	2280
120	2527
135	2748

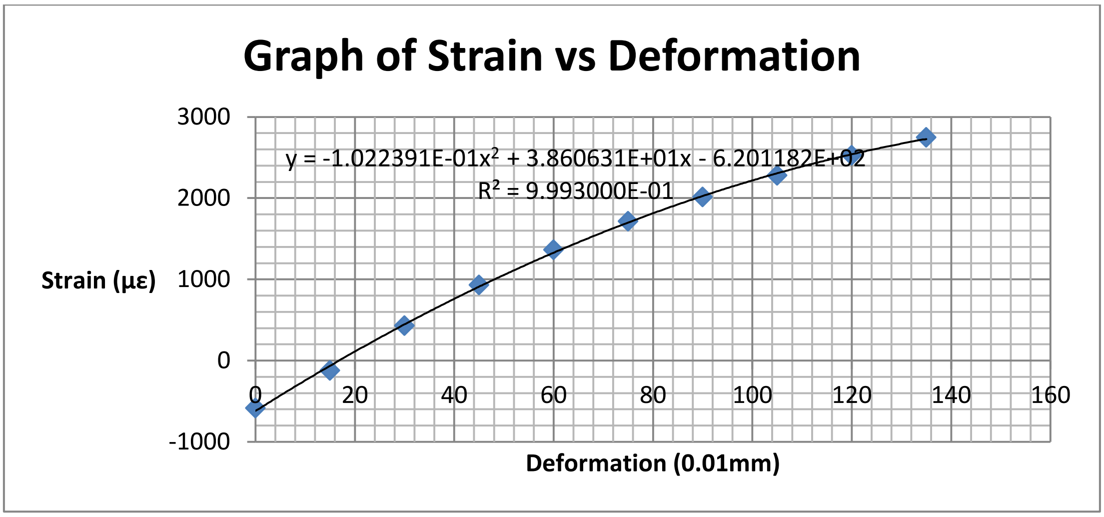

From the equation of the graph, 1 mm deformation is 2218 με.

APPENDIX G: Calibration of LDT

Case 1:

Deformation (0.01mm)	Amplified Voltage (v)
150	-9.8
145	-9.48
140	-9.23
135	-8.96
130	-8.71
125	-8.48
120	-8.21
115	-7.96
110	-7.67
105	-7.4
100	-7.14
105	-7.49
110	-7.73
115	-8.02
120	-8.29
125	-8.55
130	-8.82
135	-9.06
140	-9.28
145	-9.55
150	-9.78
145	-9.44
140	-9.23
135	-8.94
130	-8.69
125	-8.43
120	-8.17
115	-7.91
110	-7.63
105	-7.38
100	-7.09

Case 2:

Deformation (0.01mm)	Amplified Voltage (v)
100	-7.09
101	-7.2
102	-7.27
103	-7.33
104	-7.37
105	-7.44
106	-7.49
107	-7.55
108	-7.6
109	-7.67
110	-7.73
109	-7.63
108	-7.55
107	-7.49
106	-7.42
105	-7.37
104	-7.32
103	-7.25
102	-7.21
101	-7.14
100	-7.08

Case 1 is for large strain calibration and Case 2 is for small strain calibration.

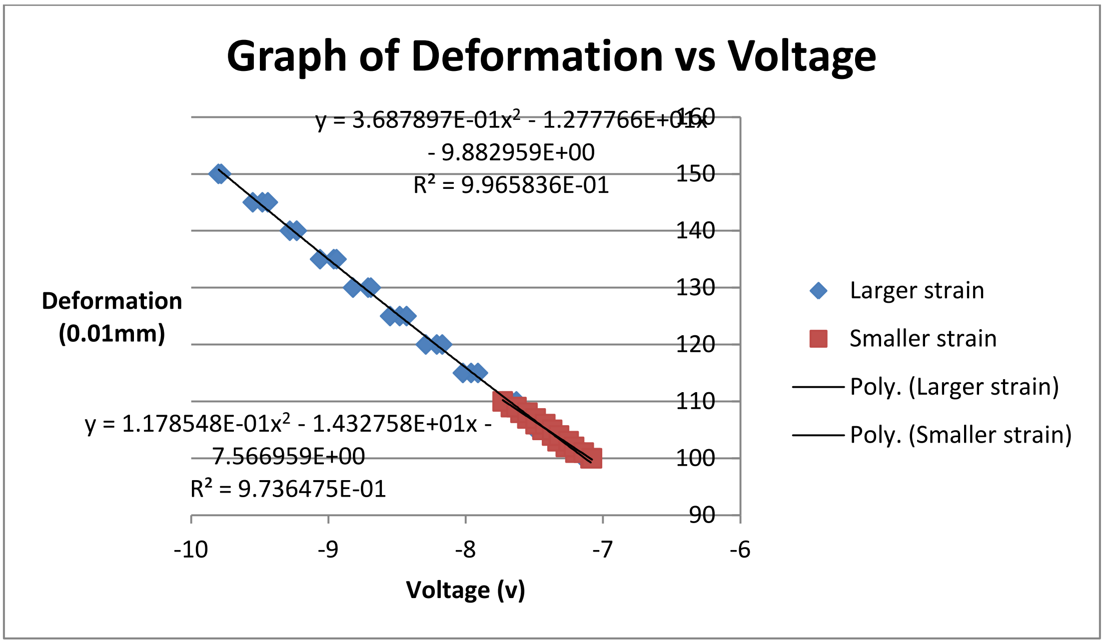

APPENDIX H: Test Specimen Data

		Unit
Density	16	kN/m3
Diameter	100	mm
Heigh	200	mm
Volume	1570796	mm3
	0.001571	m3
Area	7853.982	mm2
	0.007854	m2
Mass of soil needed	0.025133	kN
	2.513274	kg
Mass of 20% water	0.502655	kg

Specimen dimension (Before testing)

Diameter (mm)	Top	100.140000
		99.850000
	Bottom	100.450000
		99.990000
Height (mm)		200.710000
		200.400000
		199.690000
Mass (g)		3083.500000
Average Diameter (mm)		100.107500
Average Height (mm)		200.266667
Area (mm2)		7870.876771
Area (m2)		0.007871

Specimen dimension (After testing)

Diameter (mm)	Top	98.160000
		96.680000
		96.060000
	Bottom	99.190000
		100.350000
		100.330000
Height (mm)		199.690000

	200.340000
	199.670000
Average Diameter (mm)	98.461667
Average Height (mm)	199.900000
Area (mm2)	7614.199420
Area (m2)	0.007614

Moisture content after testing:

Mass of empty tray (g)	34.1
Mass of tray with wet soil (g)	184
Mass of tray with dry soil (g)	155.8
Mass of water content (g)	28.2
Mass of wet soil (g)	149.9
Moisture content (%)	18.81254

Stress ratio	Deviatoric stress	Pressure	Load	Pressure gauge	From DAQ (amplitude)
(σd/2)/σc	σd (Kpa)	kg/m2	kg	bar	V
0.01	2	200	1.570796327	0.033577347	0.041354566
0.02	4	400	3.141592654	0.067154695	0.082709132
0.05	10	1000	7.853981634	0.167886737	0.206772831
0.07	14	1400	10.99557429	0.235041432	0.289481963
0.1	20	2000	15.70796327	0.335773474	0.413545662
0.12	24	2400	18.84955592	0.402928169	0.496254794
0.15	30	3000	23.5619449	0.503660211	0.620318493
0.2	40	4000	31.41592654	0.671546948	0.827091324
0.25	50	5000	39.26990817	0.839433685	1.033864154
0.3	60	6000	47.1238898	1.007320422	1.240636985
0.35	70	7000	54.97787144	1.175207159	1.447409816
0.4	80	8000	62.83185307	1.343093896	1.654182647

APPENDIX I: Consolidation Data

Time (s)	0	15	30	60	90	120
LVDT (v)	0.65	1.37	1.39	1.39	1.39	1.39
LDT (v)	-5.33	-8.16	-8.17	-8.12	-8.13	-8.13

Time (s)	180	240	360	480	600	900
LVDT (v)	1.4	1.4	1.4	1.41	1.41	1.41
LDT (v)	-8.14	-8.14	-8.13	-8.11	-8.09	-8.02

Time (s)	1200	1500	1800	2400	3000	3600
LVDT (v)	1.41	1.41	1.41	1.41	1.41	1.41
LDT (v)	-7.95	-7.89	-7.83	-7.7	-7.66	-7.63

Time (s)	4200	4800	5400	6000	6600	7200	7800
LVDT (v)	1.41	1.41	1.41	1.41	1.41	1.41	1.41
LDT (v)	-7.61	-7.6	-7.58	-7.56	-7.55	-7.54	-7.53

Δ Deformation	-2.2	v
Δ Deformation	0.245241	mm
Strain	0.001227	
Initial Area	0.007614	m2
Final Area	0.007595	m2

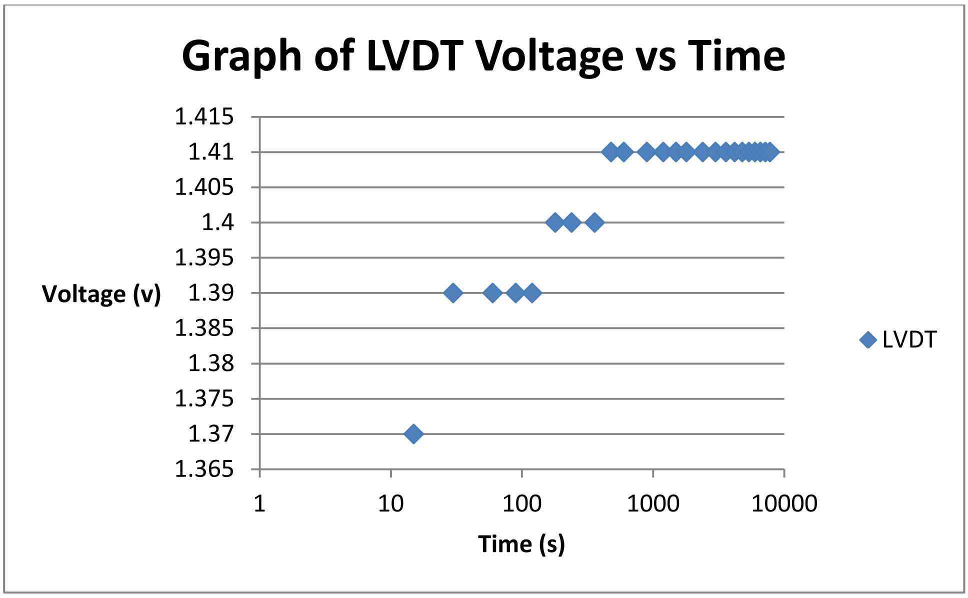
Graph of LVDT Voltage vs Time
1.415
1.41
1.405
1.4
1.395
1.39
1.385
1.38
1.375
1.37
1.365
Voltage (v)
1
10
100
1000
10000
Time (s)
LVDT

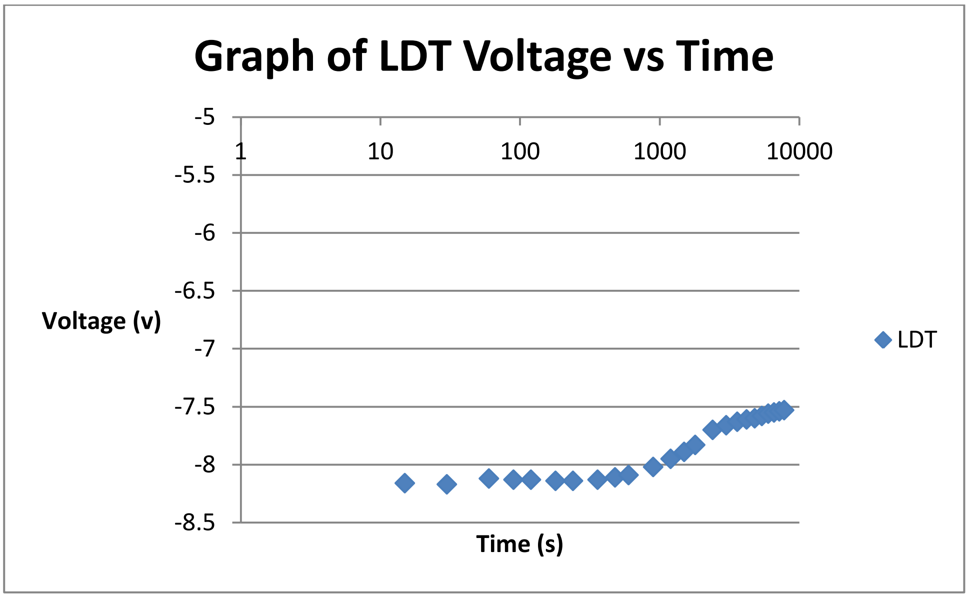
Graph of LDT Voltage vs Time
-5
-5.5
-6
-6.5
-7
-7.5
-8
-8.5
Voltage (v)
1
10
100
1000
10000
Time (s)
LDT